TECHNICAL REPORT

WVT-7102

HEAT TRANSFER BY RADIATION AND CONVECTION FROM ANNULAR FINS OF TRAPEZOIDAL PROFILE ON A CYLINDER

BY

GARRY C. CAROFANO

AND

MANUEL V. AVILA

JANUARY 1971

BENET R&E LABORATORIES

WATERVLIET ARSENAL

WATERVLIET—NEW YORK

AMCMS No. 5523.11.50300.01

DA PROJECT NO. 1W562603A209

90

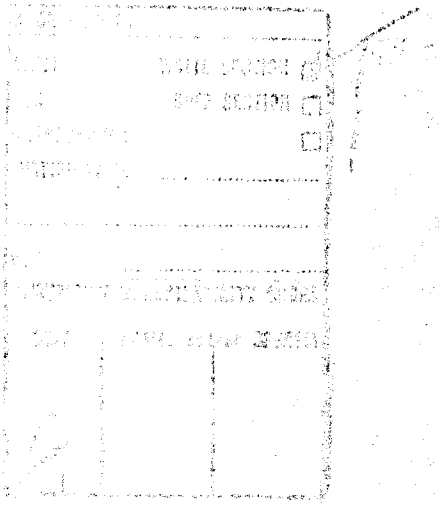

DISPOSITION

Destroy this report when it is no longer needed. Do not return it to the originator.

DISCLAIMER

The findings in this report are not to be construed as an official Department of the Army position.

Unclassified
Security Classification

DOCUMENT CONTROL DATA - R & D

(Security classification of title, body of abstract and indexing annotation must be entered when the overall report is classified)

1. ORIGINATING ACTIVITY *(Corporate author)*

Watervliet Arsenal
Watervliet, N.Y. 12189

2a. REPORT SECURITY CLASSIFICATION

Unclassified

2b. GROUP

3. REPORT TITLE

HEAT TRANSFER BY RADIATION AND CONVECTION FROM ANNULAR FINS OF TRAPEZOIDAL PROFILE ON A CYLINDER

4. DESCRIPTIVE NOTES *(Type of report and inclusive dates)*

Technical Report

5. AUTHOR(S) *(First name, middle initial, last name)*

Garry C. Carofano
Manuel V. Avila

6. REPORT DATE	7a. TOTAL NO. OF PAGES	7b. NO. OF REFS
January 1971	82	11

8a. CONTRACT OR GRANT NO.	9a. ORIGINATOR'S REPORT NUMBER(S)
AMCMS No. 5523.11.58300.01	
b. PROJECT NO. DA Project No. 1W562603A299	WVT-7102
c.	9b. OTHER REPORT NO(S) *(Any other numbers that may be assigned this report)*
d.	

10. DISTRIBUTION STATEMENT

This document has been approved for public release and sale; its distribution is unlimited.

11. SUPPLEMENTARY NOTES	12. SPONSORING MILITARY ACTIVITY
	U. S. Army Weapons Command

13. ABSTRACT

The equations describing steady heat transfer by radiation and convection from annular fins of trapezoidal profile on a cylinder are derived. Mutual irradiation between adjacent fins is considered and the appropriate differential angle factors are presented. A constant convection coefficient is assumed over all surfaces and the fins are treated as gray body radiators. The governing integral equations are approximated by numerical quadrature formulas and the resulting set of non-linear algebraic equations is programmed for solution. A Fortran program listing is included. Some results are obtained for the XM144E1 mortar tube.

DD FORM 1 NOV 68 1473 REPLACES DD FORM 1473, 1 JAN 64, WHICH IS OBSOLETE FOR ARMY USE.

Unclassified
Security Classification

14. KEY WORDS	LINK A		LINK B		LINK C	
	ROLE	WT	ROLE	WT	ROLE	WT
Heat Transfer						
Steady State						
Fins						
Cylinder						
Conduction						
Convection						
Radiation						

HEAT TRANSFER BY RADIATION AND CONVECTION FROM ANNULAR FINS OF TRAPEZOIDAL PROFILE ON A CYLINDER

ABSTRACT

The equations describing steady heat transfer by radiation and convection from annular fins of trapezoidal profile on a cylinder are derived. Mutual irradiation between adjacent fins is considered and the appropriate differential angle factors are presented. A constant convection coefficient is assumed over all surfaces and the fins are treated as gray body radiators. The governing integral equations are approximated by numerical quadrature formulas and the resulting set of non-linear algebraic equations is programmed for solution. A Fortran program listing is included. Some results are obtained for the XM144E1 mortar tube.

Key Words

Heat Transfer
Steady State
Fins
Cylinder
Conduction
Convection
Radiation

TABLE OF CONTENTS

TABLE OF CONTENTS (CONT'D)

FIGURES

FIGURES (CONT'D)

GLOSSARY

A description of the most frequently used symbols is given below. The remaining symbols used in the text are defined when they are introduced.

SYMBOL	DESCRIPTION
h	Convective film coefficient [Btu/hr-ft^2-°R]
h^*	Convection parameter $\left[= \dfrac{h\, R_i^2}{k_m \cos\alpha\,(\delta + (R_o - R_i)\tan\alpha)} \right]$
k_a	Thermal conductivity of air [Btu/hr-ft-°R]
k_m	Thermal conductivity of fin material [Btu/hr-ft-°R]
L	Distance between fin tips [ft]
N_c	Radiation parameter $\left[= \dfrac{R_i^2\, \sigma\, T_b^3}{k_m \cos\alpha\,(\delta + (R_o - R_i)\tan\alpha)} \right]$
N_L	Dimensionless parameter [$= L/R_o$]
N_R	Dimensionless parameter [$= R_i/R_o$]
q_T	Total heat transfer rate [Btu/hr]
$\bar{q}_T$	Total heat transfer rate per unit length [Btu/hr-ft]
$q(r)$	Local fin radiative heat flux [Btu/hr-ft^2]
$q_b(z_b)$	Local base radiative heat flux [Btu/hr-ft^2]
$Q(\varrho)$	Dimensionless variable [$= q(r)/\sigma T_b^4$]
$\phi_b(\tau_b)$	Dimensionless variable [$= q_b(z_b)/\sigma T_b^4$]
r	Radial coordinate [ft]
R_i	Base cylinder radius [ft]
R_o	Fin tip radius [ft]
S	Fin spacing [$= L + 2\,\delta$]
S_o	Fin spacing on XM144E1 mortar [see Figure 1]

SYMBOL	DESCRIPTION
T_b	Base cylinder temperature [°R, unless otherwise noted]
T_e	Environment temperature [°R, unless otherwise noted]
T_e^*	Dimensionless parameter [$= T_e/T_b$]
T(r)	Local fin temperature [°R]
$T^*(\rho)$	Dimensionless variable [$= T(r)/T_b$]
z_b	Longitudinal coordinate [ft]

GREEK SYMBOLS

α	Fin angle [degrees]
δ	Fin tip half-thickness [ft]
δ^*	Dimensionless parameter [$= \delta/R_o$]
ϵ	Emissivity
ρ	Dimensionless variable [$= r/R_o$]
β	Fin system effectiveness
σ	Stefan-Boltzmann constant [1.714×10^{-9} Btu/hr-ft^2-°R^4]
τ_b	Dimensionless variable [$= z_b/R_o$]

SUBSCRIPTS

1	Refers to fin 1
2	Refers to fin 2
b	Refers to base cylinder
e	Refers to environment

INTRODUCTION

As an aid in formulating the present problem some of the thermal operating characteristics of mortars will first briefly be reviewed.

When a mortar is fired a fraction of the chemical energy released in the propellant combustion process is absorbed as thermal energy at the bore surface. In a cold weapon a portion of this energy is retained by the barrel in the form of internal energy; the remainder is conducted through the tube wall and dissipated at the outer surface by convective and radiative exchange with the surroundings. In a sustained firing situation the energy storage results in an increase in average barrel temperature, although, for moderate firing rates, a quasi-steady radial temperature distribution eventually develops through a major portion of the tube wall; the rate of energy input at the bore surface is then just balanced by the dissipation rate at the outer surface.

Also characteristic is the development of an appreciable non-uniformity of temperature in the axial direction which is related to the complicated nature of the internal gas flow; the axial temperature distribution increases with distance from the breech, attains a maximum and then decreases monotonically towards the muzzle. This distribution also becomes approximately steady with time in the outer regions of the barrel wall.

The design of a mortar is controlled to a considerable extent by the mechanical and thermal behavior of the tube segment located in the vicinity of the axial temperature maximum. It is at this point that the tube strength is at a minimum because of the inverse relationship between temperature and the mechanical properties of the material. Through a suitable failure

criterion the internal gas pressure and the tube wall-ratio can be related to the yield stress of the material. Since the latter quantity has a unique dependence on temperature, the maximum sustained operating temperature which can be permitted is that corresponding to the minimum yield stress which will just maintain the structural integrity of the tube under the specified internal loading conditions. The maximum heat dissipation rate at the outer surface is also determined by this particular value of temperature and, since this is balanced by the energy input at the bore surface, a maximum firing rate is implied.

It would be desirable to design a mortar with a permissable firing rate which exceeds the maximum rate at which individuals could load it. Although this goal is far from being attained by present day mortars, significant advances have been made by increasing the heat transfer rate from the outer surface through the additions of fins. An example of such a design is the XM144E1 mortar, a section of which is shown in Figure 1. The problem is to optimize the firing rate (i.e., heat transfer rate) for a given tube weight.

The addition of fins to the surface of a tube seriously complicates the calculation of heat transfer. Conduction of energy within the fin must be calculated simultaneously with the radiative and convective losses at the fin surface. Mutual irradiation between adjacent fins and between the fins and the tube surface must also be considered. By contrast, the radiative and convective heat transfer rates from a smooth cylinder are independent of each other and may be evaluated from relatively simple expressions.

Finning also complicates the prediction of tube strength although it should be noted that annular fins contribute significantly to the load carrying capacity of the tube. For a given internal pressure, a properly designed finned tube has a smaller wall-ratio than a structurally equivalent smooth tube, although the overall tube weight per unit length is slightly higher in the former case. Thus, the weight penalty incurred with the addition of annular fins is less than the actual weight of material making up the fins.

The problem facing the designer can be stated as follows: for a given weight addition of material per unit tube length, maximize the heat dissipating ability of the outer surface while simultaneously maintaining the structural integrity of the tube under the specified loading conditions. The heat transfer rate and the tube section strength must be considered together since they are related through the maximum allowable material temperature and the tube geometry -- that is, the tube wall-ratio and the spacing, height and profile of the fins.

A desirable design tool would appear to be a computer program which accepts as input such basic parameters as weapon caliber, internal peak pressure, material properties -- that is, the thermal conductivity, surface radiative emissivity and yield stress, all at the maximum tube temperature -- and the maximum tube weight per unit length. Output would be the tube geometry and the optimized heat transfer rate per unit tube length.

Information in two areas is required. First, an empirical relationship must be found which relates tube strength and material yield stress to an arbitrary fin-tube geometry. This information can be obtained, for example,

through a parametric photoelastic study of various fin-tube sections. Secondly, the ability to predict the heat transfer rate from an arbitrary tube geometry is necessary. Empirical information on the convective heat transfer coefficient as well as a mathematical model of the combined radiation-convection problem must be obtained. The latter problem, along with a cursory examination of the optimization problem, will be treated in this report. The photoelastic and convection studies will be the subject of future proposed work.

PROBLEM STATEMENT

The quasi-steady nature of the temperature distribution on the outer barrel surface permits a steady-state heat transfer analysis to be made. Furthermore, the spatial temperature variation in the axial direction can be taken into account, when desired, by subdividing the tube into sections along its axis and assigning each section an average constant temperature over its length. The segment containing the temperature maximum is of primary interest here.

The tube geometry can be approximated as shown in Figure 1. An actual mortar design, of course, would have fillets at the intersection of the fins and the tube and, although this would be an important consideration in regard to tube strength, it is not expected to substantially alter the heat transfer prediction. Thus, the problem reduces to an analysis of the combined steady convective and radiative heat transfer from an ensemble of annular fins of trapezoidal profile on a circular isothermal tube.

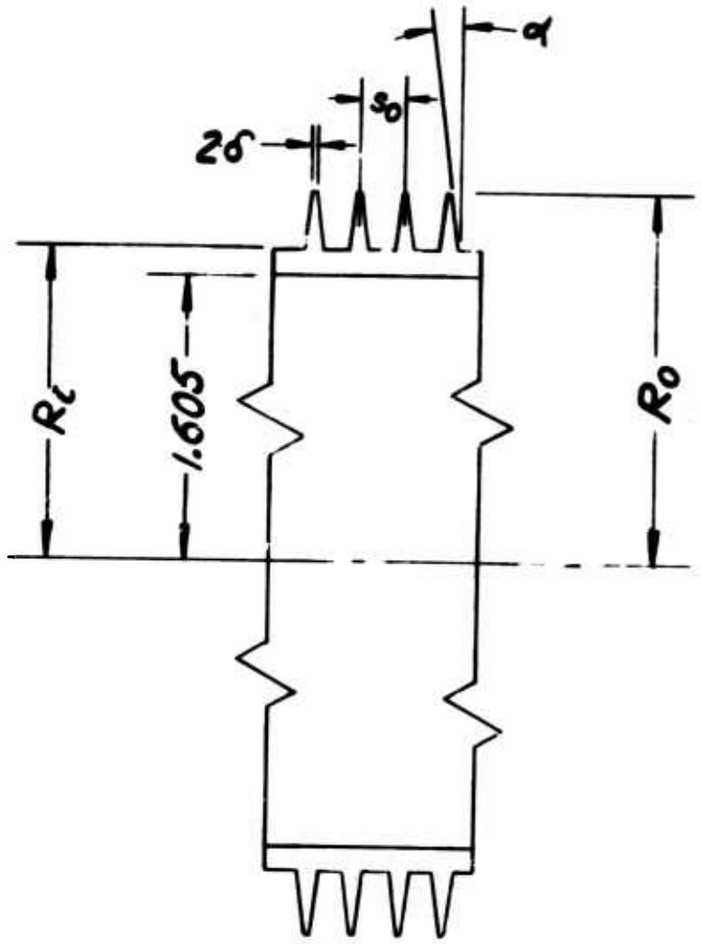

$s_0 = .250$
$\alpha = 7.25°$
$R_0 = 2.064$
$R_i = 1.730$
$\delta = 0.015$

FIGURE 1. FIN CONFIGURATION USED ON XM144E1 MORTAR TUBE.

Convective transfer from annular fins of various profiles has been summarized by Kraus [1].* Radiative transfer from fins of uniform profile was studied by Sparrow, Miller and Jonsson [2]. Their analysis included the complicated radiative interaction between a fin and the tube base as well as mutual irradiation between adjacent fins. Edwards and Chaddock [3] extended the treatment to include convection but limited their calculations to specific fin materials and tube temperatures. Dent [4] treated the same problem but confined his work to a method of solution rather than a presentation of design information. Recently, Keller and Holdredge [5] presented results for radiative transfer from a single annular fin of trapezoidal profile. Convection and incident radiation upon the fin surface were not included in their analysis. The present study, therefore, represents an extension of these analyses.

ANALYSIS

Basic Assumptions. The configuration to be analyzed is shown in Figure 2. The nomenclature is shown in the upper portion of the figure. The non-dimensionalized variables shown in the lower portion of the figure will be defined later.

Because an ensemble of fins on an isothermal surface is assumed only the center-line to center-line distance between any two adjacent fins has to be considered. It is further assumed that:

1. Conduction of heat within the fin is one-dimensional and steady.
2. The fin and tube surfaces are gray diffuse reflectors and emitters

* Numbers in brackets designate references at end of report.

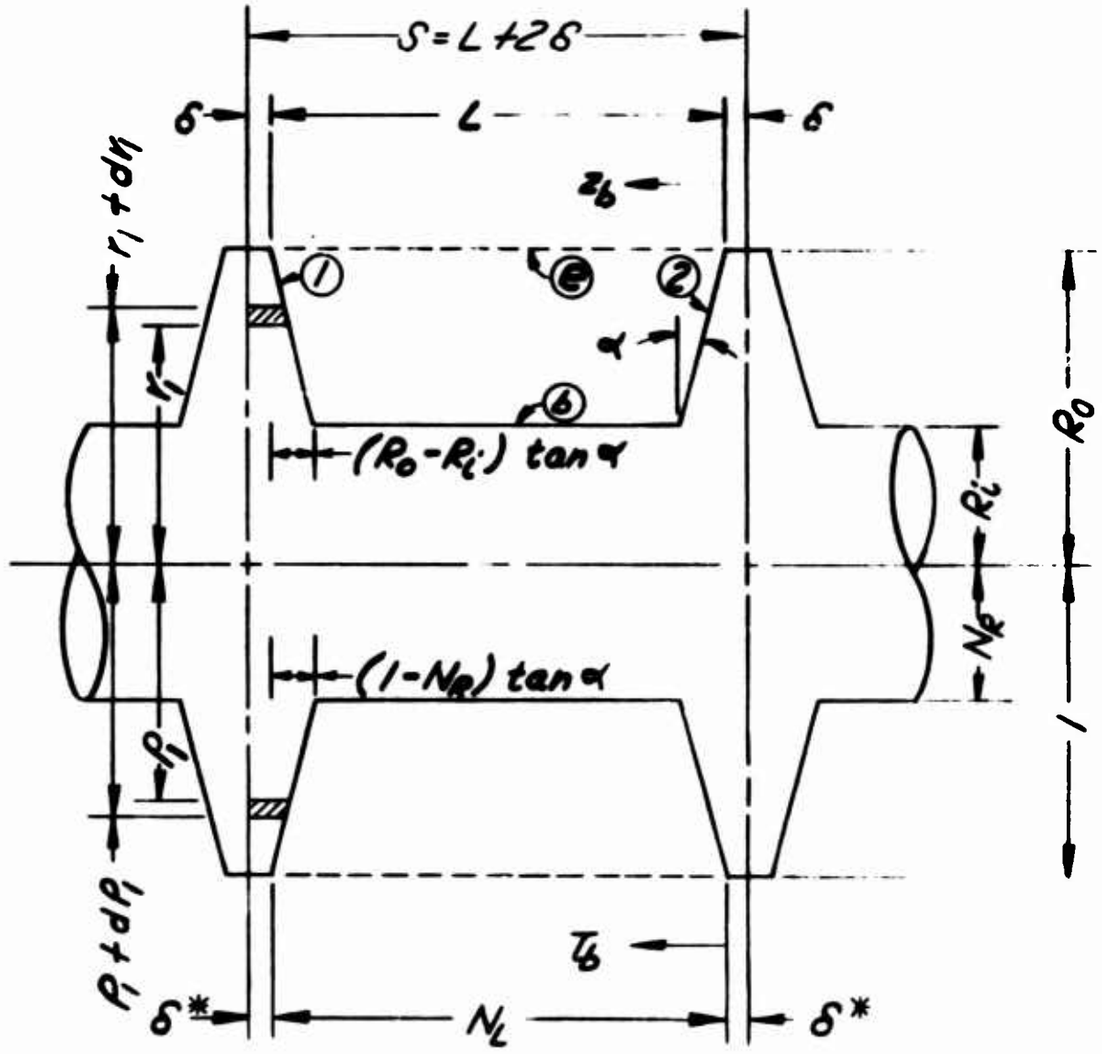

FIGURE 2. NOMENCLATURE USED IN THE ANALYSIS.

with constant emissivity, ϵ.

3. A constant convective film coefficient, h, prevails over all surfaces.

4. The radiation from the environment can be characterized as coming from a black body source at temperature T_e, equal to that of the surrounding medium.

5. The fin base and tube surface have the same constant temperature, T_b.

6. The thermal conductivity of the fin material, k_m, is a constant.

Energy Equation. Consider the incremental volume shown in Figure 2 located between r_1 and $r_1 + dr_1$. On the fin surface this volume element has a surface area $dA_1^* = r_1 d\theta dr_1/\cos\alpha$ where $r_1 d\theta$ is the width of the element and $dr_1/\cos\alpha$ is the height (see Figure 3). Energy is conducted into the element at r_1. It loses energy by conduction at $r_1 + dr_1$ and by convection and radiation at its surface, dA_1^*. An energy balance gives

$$\frac{d}{dr_1}\left[k_m r_1 [\delta + (R_o - r_1)\tan\alpha] \frac{dT_1(r_1)}{dr_1} \right] d\theta dr_1$$

$$= q_1(r_1) \frac{r_1 d\theta dr_1}{\cos\alpha} + h[T_1(r_1) - T_e] \frac{r_1 d\theta dr_1}{\cos\alpha} \qquad (1)$$

The term on the left represents the net energy conducted <u>into</u> the element per unit time. The variable fin thickness is $[\delta + (R_o - r_1)\tan\alpha]$ and k_m is the material thermal conductivity.

The first term on the right represents the net energy <u>lost</u> by radiation from the element per unit time. $q_1(r_1)$ is the radiative heat transfer per unit area per unit time at r_1. The second term represents the convective

loss due to the temperature difference $[T_1(r_1) - T_e]$ between the fin and the surrounding medium.

Equation (1) is a second-order ordinary differential equation involving two unknown functions, $T_1(r_1)$ and $q_1(r_1)$. An appropriate equation will be derived in the next section for the radiative flux, $q_1(r_1)$. Of the two boundary conditions required on $T_1(r_1)$ the first is given by assumption (5) above which states that the fin base temperature is equal to the tube temperature, T_b, or

$$T_1(r_1) = T_b \qquad \text{at } r_1 = R_i \tag{2}$$

The second boundary condition is obtained by equating the energy conducted to the fin tip area, $\delta R_o d\theta$, to the energy lost by convection and radiation from this surface, or

$$-k_m \frac{dT_1(r_1)}{dr_1} \delta R_o d\theta = h[T_1(r_1) - T_e]\, \delta R_o d\theta + \varepsilon[\sigma T_1^4(r_1) - \sigma T_e^4]\, \delta R_o d\theta \qquad \text{at } r_1 = R_o \tag{3}$$

A similar procedure could be followed for the temperature distribution $T_2(r_2)$ in the opposite fin, but, due to symmetry, $T_2(r_2)$ is identical to the function $T_1(r_1)$ when $r_2 = r_1$, hence, the resulting equation would be redundant.

Radiation Equations. Attention will now be directed to the determination of the radiative flux term, $q_1(r_1)$, in equation (1). The net radiation per unit area per unit time leaving the surface element dA_1^* is equal the energy emitted from this surface, by virtue of its temperature, less the energy absorbed. The latter quantity includes contributions from the surroundings, the opposite

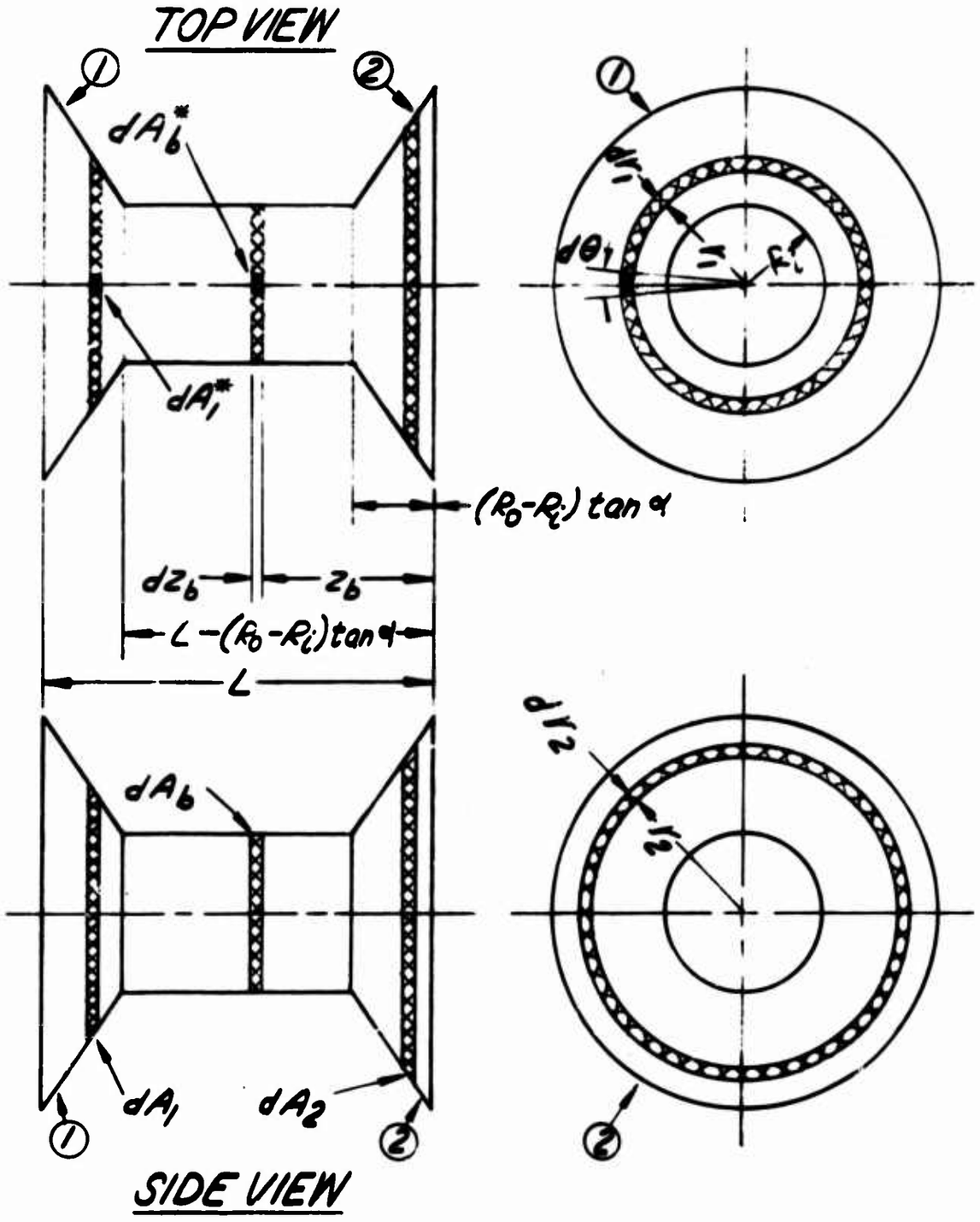

FIGURE 3. ELEMENTAL AREAS USED IN RADIATIVE ANALYSIS.

fin and the tube surface. It also includes energy originally emitted by dA_1^* and arriving back at this surface after reflections off the opposite fin and tube surfaces when these surfaces are not black (i.e., $\epsilon<1$). The complex radiation balance is most easily made by employing enclosure theory and the concept of radiosity [see ref. 6, Chapter 3].

The enclosure to be analyzed is shown in Figures 2 and 3. It consists of the conical surfaces of two adjacent fins, designated by the subscripts "1" and "2", the cylindrical base surface between the fins, designated by the subscript "b", and the inner surface of the fictitious cylindrical sheath stretched across the opening shown in Figure 2 and designated by the subscript "e". As noted earlier, this sheath is treated as a black body with an effective temperature, T_e.

The term "radiosity" refers to the total energy per unit area per unit time leaving a surface. It is equal to the sum of the diffusely emitted and diffusely reflected radiation and may be written as

$$B_i(\underline{r}_i) = \epsilon_i \sigma T_i^4(\underline{r}_i) + (1-\epsilon_i)H_i(\underline{r}_i) \qquad (4)$$

The subscript "i" designates the i-th surface of the enclosure and the vector $\underline{r}_i$ designates the position of an element on this surface with respect to some convenient coordinate system. The first term on the right-hand side of eq. (4) represents the rate at which energy is emitted per unit area per unit time; ϵ_i is the emissivity of the i-th surface. The symbol $H_i(\underline{r}_i)$ is called the "irradiation" and refers to all radiation incident at $\underline{r}_i$ per unit area per unit time. The term $(1-\epsilon_i)$ represents the reflectivity of a gray surface and the product $(1-\epsilon_i)H_i(\underline{r}_i)$ is the energy per unit area per unit time diffusely reflected from the surface at $\underline{r}_i$.

Since the radiosity, $B_i(\underline{r}_i)$, is assumed to be diffusely distributed, the concept of the angle factor can be employed [see ref. 6, Chapter 4]. In particular, the notation $dF(\underline{r}_i, \underline{r}_j)_{dA_i^*-dA_j}$ will be used to designate the fraction of the energy leaving surface element dA_i^* located on the i-th surface at $\underline{r}_i$ and arriving at dA_j located on the j-th surface at $\underline{r}_j$. The asterisk on dA_i^* is used to denote a "second-order" differential area such as dA_1^* in Figure 3; that is, $dA_1^* = r_1 d\theta dr_1/\cos\alpha$. When the asterisk is omitted, a "first-order" differential area is implied; for example, $dA_2 = 2\pi r_2\, dr_2/\cos\alpha$.

The notation $F(\underline{r}_i)_{dA_i^*-A_j}$ will be used to designate the fraction of the energy leaving surface element dA_i^* which is intercepted by the entire surface A_j. The following "reciprocity rules" are derived in ref. 6 and will be used in the development below.

$$dA_i^* dF(\underline{r}_i, \underline{r}_j)_{dA_i^*-dA_j} = dA_j dF(\underline{r}_j, \underline{r}_i)_{dA_j-dA_i^*} \tag{5}$$

$$dA_i^* F(\underline{r}_i)_{dA_i^*-A_j} = A_j F(\underline{r}_i)_{A_j-dA_i^*} \tag{6}$$

The expression for the energy incident on dA_1^* will now be derived. Consider first the contribution from the opposite fin. The total energy per unit time leaving the ring element dA_2 located at r_2 in Figure 3 is $B_2(r_2)dA_2$. Of this amount the fraction $dF(r_2, r_1)_{dA_2-dA_1^*}$ arrives at dA_1^* or

$$B_2(r_2)dA_2 dF(r_2, r_1)_{dA_2-dA_1^*}$$

The total irradiation of dA_1^* from the opposite fin is found by summing the contributions of all of the ring elements on A_2 with the result

$$\int_{R_i}^{R_o} B_2(r_2)\,dA_2\,dF(r_2,\, r_1)_{dA_2\text{-}dA_1^*}$$

Specializing eq. (5) to this situation gives

$$dA_2\,dF(r_2,\, r_1)_{dA_2\text{-}dA_1^*} = dA_1^*\,dF(r_1,\, r_2)_{dA_1^*\text{-}dA_2}$$

Using this result in the above integral gives

$$dA_1^* \int_{R_i}^{R_o} B_2(r_2)\,dF(r_1,\, r_2)_{dA_1^*\text{-}dA_2}$$

where dA_1^* has been removed from under the integral sign since it is independent of the integration variable r_2.

A similar procedure can be followed to calculate the irradiation of dA_1^* by all ring elements dA_b on the tube surface with the result

$$dA_1^* \int_{(R_o - R_i)\tan\alpha}^{L - (R_o-R_i)\tan\alpha} B_b(z_b)\,dF(r_1,\, z_b)_{dA_1^*\text{-}dA_b}$$

$B_b(z_b)$ is the radiosity of the ring element dA_b located at z_b on the tube surface. Note the asymmetric origin of the z_b-coordinate in Figure 2 and note also that the tube surface extends from $z_b = (R_o-R_i)\tan\alpha$ to $z_b = L - (R_o-R_i)\tan\alpha$.

Since the surface A_e is assumed to behave as a black body with uniform temperature, T_e, its emissivity is unity and, by eq. (4), its radiosity is

simply $B_e = \sigma T_e^4$, independent of position. The total energy emitted by A_e is $\sigma T_e^4 A_e$ and the fraction

$$\sigma T_e^4 A_e dF(r_1)_{A_e - dA_1^*}$$

is intercepted by dA_1^*. Using the reciprocity rule in eq. (6) this quantity can also be written as

$$\sigma T_e^4 dA_1^* F(r_1)_{dA_1^* - A_e}$$

Since surface "1" is convex it does not irradiate itself, so the total energy per unit time incident on dA_1^* is the sum of the three contributions above. Dividing this sum by dA_1^* the irradiation per unit area per unit time is obtained, that is, $H_1(r_1)$. Thus,

$$H_1(r_1) = \int_{R_i}^{R_o} B_2(r_2) dF(r_1, r_2)_{dA_1^* - dA_2}$$

$$+ \int_{(R_o - R_i)\tan\alpha}^{L - (R_o - R_i)\tan\alpha} B_b(z_b) dF(r_1, z_b)_{dA_1^* - dA_b} + \sigma T_e^4 F(r_1)_{dA_1^* - A_e} \qquad (7)$$

The net local radiation flux is given by

$$q_i(r_i) = \varepsilon_i \sigma T_i^4(r_i) - \varepsilon_i H_i(r_i) \qquad (8)$$

The second term on the right-hand side of eq. (8) represents the fraction of the incident energy which is absorbed; by the gray body assumption the absorbtivity is equal to the emissivity, ε_i.

Eliminating $H_i(r_i)$ in eqs. (4) and (8) gives

$$\epsilon_i B_i(\underline{r}_i) = \epsilon_i \sigma T_1^4(\underline{r}_i) - (1 - \epsilon_i) q_i(\underline{r}_i) \tag{9}$$

Using this expression to eliminate $B_2(r_2)$ and $B_b(z_b)$ in eq. (7) and substituting the result into eq. (8) gives

$$q_1(r_1) = \epsilon\sigma T_1^4(r_1) - \int_{R_i}^{R_o} [\epsilon\sigma T_2^4(r_2) - (1-\epsilon) q_2(r_2)] dF(r_1, r_2)_{dA_1^*-dA_2}$$

$$- \int_{(R_o-R_i)\tan\alpha}^{L-(R_o-R_i)\tan\alpha} [\epsilon\sigma T_b^4 - (1-\epsilon) q_b(z_b)] dF(r_1, z_b)_{dA_1^*-dA_b} - \epsilon\sigma T_e^4 F(r_1)_{dA_1^*-A_e} \tag{10}$$

Due to symmetry the expression for $q_2(r_2)$ can be obtained by simply interchanging the subscripts "1" and "2" in the above equation. Also, note that the tube surface temperature, T_b, is not a function of position (see assumption (5) above).

An analogous procedure yields the following expression for the base radiative flux:

$$q_b(z_b) = \epsilon\sigma T_b^4 - \int_{R_i}^{R_o} [\epsilon\sigma T_1^4(r_1) - (1-\epsilon) q_1(r_1) dF(z_b, r_1)_{dA_b^*-dA_1}$$

$$- \int_{R_i}^{R_o} [\epsilon\sigma T_2^4(r_2) - (1-\epsilon) q_2(r_2)] dF(z_b, r_2)_{dA_b^*-dA_2} - \epsilon\sigma T_e^4 F(z_b)_{dA_b^*-A_e} \tag{11}$$

Note that while the tube emits energy uniformly over its surface by virtue of its constant temperature, the irradiation, denoted by the last three terms in eq. (11), is a function of position. Finally, because the tube is a convex surface it does not irradiate itself.

Eqs. (10) and (11) can be simplified considerably by taking advantage of certain symmetries in the problem and through the use of angle factor algebra. As noted earlier, due to symmetry, the functions $T_2(r_2)$ and $q_2(r_2)$ are identical to the functions $T_1(r_1)$ and $q_1(r_1)$ when $r_2 = r_1$. Also, the angle factor $dF(z_b, r_2)_{dA_b^* - dA_2}$ may be replaced by $dF(L-z_b, r_1)_{dA_b^* - dA_1}$ when $r_2 = r_1$. The latter angle factor is evaluated at $(L-z_b)$ rather than z_b because the fins are not symmetrically located about the z_b origin (see Figure 2). Finally, the following angle factor relationships apply:

$$F(r_1)_{dA_1^* - A_e} + \int_{R_i}^{R_o} dF(r_1, r_2)_{dA_1^* - dA_2} + \int_{(R_o - R_i)\tan\alpha}^{L - (R_o - R_i)\tan\alpha} dF(r_1, z_b)_{dA_1^* - dA_b} = 1 \qquad (12)$$

$$F(z_b)_{dA_b^* - A_e} + \int_{R_i}^{R_o} dF(z_b, r_1)_{dA_b^* - dA_1} + \int_{R_i}^{R_o} dF(z_b, r_2)_{dA_b^* - dA_2} = 1 \qquad (13)$$

The three terms on the left-hand side of eq. (12) represent, respectively, the fraction of the energy leaving dA_1^* which is intercepted by the sheath area, A_e, the area of the opposite fin, A_2, and the tube base area, A_b. Since these three surfaces and A_1, which does not see itself, form an enclosure, the above three fractions must sum to unity as indicated in eq. (12). A similar interpretation applies to eq. (13).

Adopting the notation

$$K_{12}(r_1, r_2) = dF(r_1, r_2)_{dA_1^* - dA_2} \quad / dr_2$$

$$K_{1b}(r_1, z_b) = dF(r_1, z_b)_{dA_1^* - dA_b} \quad / dz_b$$

$$K_{b1}(z_b, r_1) = dF(z_b, r_1)_{dA_b^* - dA_1} \Big/ dr_1$$

and using the above results, eqs. (10) and (11) become

$$q_1(r_1) = \epsilon[\sigma T_1^4(r_1) - \sigma T_e^4] - \int_{R_i}^{R_o} \{\epsilon[\sigma T_1^4(\xi) - \sigma T_e^4] - (1-\epsilon)q_1(\xi)\} K_{12}(r_1, \xi)d\xi$$

$$- \int_{(R_o-R_i)\tan\alpha}^{L-(R_o-R_i)\tan\alpha} \{\epsilon[\sigma T_b^4 - \sigma T_e^4] - (1-\epsilon)q_b(\xi)\} K_{1b}(r_1, \xi)d\xi \qquad (14)$$

$$q_b(z_b) = \epsilon[\sigma T_b^4 - \sigma T_e^4] - \int_{R_i}^{R_o} \{\epsilon[\sigma T_1^4(\xi) - \sigma T_e^4] - (1-\epsilon)q_1(\xi)\} K_{b1}(z_b, \xi)d\xi$$

$$- \int_{R_i}^{R_o} \{\epsilon[\sigma T_1^4(\xi) - \sigma T_e^4] - (1-\epsilon)q_1(\xi)\} K_{b1}(L-z_b, \xi)d\xi \qquad (15)$$

As is typical in problems of this type the kernel $K_{1b}(r_1, \xi)$ in the second integral of eq. (14) becomes indeterminate at the upper limit $[L - (R_o-R_i)\tan\alpha]$ when $r_1 = R_i$, that is, at the intersection of the fin and the base cylinder. The difficulty in evaluating the integral numerically at this point can be circumvented, however, by following a procedure given by Donovan [8] for analytically determining the integral in the limit as $r_1 \to R_i$. The details are too lengthy to be reproduced here and only the result will be quoted. Thus

$$\lim_{r_1 \to R_i} \int_{(R_o-R_i)\tan\alpha}^{L-(R_o-R_i)\tan\alpha} \{\epsilon[\sigma T_b^4 - \sigma T_e^4] - (1-\epsilon)q_b(\xi)\} K_{1b}(r_1, \xi)d\xi =$$

$$= \{\varepsilon[\sigma T_b^4 - \sigma T_e^4] - (1-\varepsilon)q_b(L - (R_o-R_i)\tan\alpha)\}(1-\sin\alpha)/2$$

A similar difficulty occurs at the lower limit in the first integral in eq. (15) as $z_b \to L - (R_o-R_i)\tan\alpha$. Analytical evaluation gives

$$\lim_{z_b \to L-(R_o-R_i)\tan\alpha} \int_{R_i}^{R_o} \{\varepsilon[\sigma T_1^4(\xi) - \sigma T_e^4] - (1-\varepsilon)q_1(\xi)\}K_{b1}(z_b,\xi)\,d\xi$$

$$= \{\varepsilon[\sigma T_b^4 - \sigma T_e^4] - (1-\varepsilon)q_1(R_i)\}(1-\sin\alpha)/2$$

where eq. (2) has been used to replace $T_1^4(R_i)$ by T_b^4 in the first term on the right-hand side of this equation.

The second integral in eq. (15) can be handled in the same manner as $z_b \to (R_o-R_i)\tan\alpha$ or advantage can be taken of the symmetry of $q_b(z_b)$ about the point $z_b = L/2$ by noting that

$$q_b((R_o-R_i)\tan\alpha) = q_b(L - (R_o-R_i)\tan\alpha)$$

One final simplification resulted after evaluation of the angle factors revealed that

$$K_{1b}(r_1, z_b) = (R_i\cos\alpha/r_1)K_{b1}(z_b, r_1)$$

Expressions for $K_{12}(r_1, r_2)$ and $K_{b1}(z_b, r_1)$ are given in Appendix A.

Non-dimensionalized Equations. The following dimensionless variables were used to non-dimensionalize the governing equation.

$$\rho_1 = \frac{r_1}{R_o} \quad , \quad \rho_2 = \frac{r_2}{R_o} \quad , \quad \tau_b = \frac{z_b}{R_o}$$

$$N_R = \frac{R_i}{R_o} \quad , \quad N_L = \frac{L}{R_o} \quad , \quad \delta^* = \frac{\delta}{R_o}$$

$$T_1^*(\rho_1) = \frac{T_1(r_1)}{T_b}, \qquad T_e^* = \frac{T_e}{T_b}$$

$$Q_1(\rho_1) = \frac{q_1(r_1)}{\sigma T_b^4}, \qquad Q_b(\tau_b) = \frac{q_b(z_b)}{\sigma T_b^4}$$

$$N_c = \frac{R_i^2 \sigma T_b^3}{k_m \cos\alpha(\delta + (R_o - R_i)\tan\alpha)}$$

$$h^* = \frac{hR_i^2}{k_m \cos\alpha(\delta + (R_o - R_i)\tan\alpha)}$$

With this notation the final form of the radiation equations becomes:

$$Q_1(N_R) = \varepsilon[1-T_e^{*4}] - \int_{N_R}^{1} \{\varepsilon[T_1^{*4}(\xi) - T_e^{*4}] - (1-\varepsilon)Q_1(\xi)\}K_{12}(N_R, \xi)d\xi$$

$$- \{\varepsilon[1-T_e^{*4}] - (1-\varepsilon)Q_b(N_L-(1-N_R)\tan\alpha)\}(1-\sin\alpha)/2 \qquad (16a)$$

$$Q_1(\rho_1) = \varepsilon[T_1^{*4}(\rho_1)-T_e^{*4}] - \int_{N_R}^{1} \{\varepsilon[T_1^{*4}(\xi)-T_e^{*4}] - (1-\varepsilon)Q_1(\xi)\}K_{12}(\rho_1,\xi)d\xi$$

$$- \frac{N_R\cos\alpha}{\rho_1} \int_{(1-N_R)\tan\alpha}^{N_L - (1-N_R)\tan\alpha} \{\varepsilon[1-T_e^{*4}] - (1-\varepsilon)Q_b(\xi)\}K_{b1}(\xi, \rho_1)d\xi \qquad (16b)$$

$$Q_b(N_L-(1-N_R)\tan\alpha) = \varepsilon[1-T_e^{*4}] - \{\varepsilon[1-T_e^{*4}] - (1-\varepsilon)Q_1(N_R)\}(1-\sin\alpha)/2$$

$$- \int_{N_R}^{1} \{\varepsilon[T_1^{*4}(\xi)-T_e^{*4}] - (1-\varepsilon)Q_1(\xi)\}K_{b1}((1-N_R)\tan\alpha, \xi)d\xi \qquad (17a)$$

$$Q_b((1-N_R)\tan\alpha) = Q_b(N_L-(1-N_R)\tan\alpha) \tag{17b}$$

$$Q_b(\tau_b) = \varepsilon[1-T_e^{*4}] - \int_{N_R}^{1} \{\varepsilon[T_1^{*4}(\xi)-T_e^{*4}] - (1-\varepsilon)Q_1(\xi)\}[K_{b1}(\tau_b, \xi) + K_{b1}(N_L-\tau_b,\xi)]d\xi \tag{17c}$$

The conduction equation and its boundary conditions become

$$\frac{d}{d\zeta_1}\left[P(\zeta_1)\frac{dT_1^*(\zeta_1)}{d\zeta_1}\right] = \frac{\zeta_1}{N_R^2}\{N_c Q_1(\zeta_1) + h^*[T_1^*(\zeta_1) - T_e^*]\} \tag{18a}$$

where

$$P(\zeta_1) = \frac{\zeta_1(\delta^* + (1-\zeta_1)\tan\alpha)}{\delta^* + (1-N_R)\tan\alpha}$$

$$T_1^*(\zeta_1) = 1 \qquad \text{at } \zeta_1 = N_R \tag{18b}$$

$$C = -\frac{dT_1^*(\zeta_1)}{d\zeta_1} = \{h^*[T_1^*(\zeta_1) - T_e^*] + \varepsilon N_c[T_1^{*4}(\zeta_1)-T_e^{*4}]\} \times \frac{[\delta^* + (1-N_R)\tan\alpha]\cos\alpha}{N_R^2} \quad \text{at } \zeta_1 = 1 \tag{18c}$$

Method of Solution. Following a technique suggested by Glauz [7] and successfully applied by Donovan [8] to the related problem of uniform fins on a plane wall, eq. (18a) was transformed into an equivalent integral equation by direct integration and application of the boundary conditions. The result is

$$T_1^*(\zeta_1) = \frac{1}{P(\zeta_1)} \left[(N_R - \zeta_1) \int_{\zeta_1}^{1} \psi(\varepsilon)\,d\varepsilon + \int_{N_R}^{\zeta_1} \phi(\varepsilon)\,d\varepsilon + N_R \right.$$
$$\left. + \frac{(N_R - \zeta_1)\delta^* C}{\delta^* + (1-N_R)\tan\alpha} \right] \qquad (19)$$

where

$$\psi(\varepsilon) = (\varepsilon/N_R^2)\{N_C Q_1(\varepsilon) + h^*[T_1^*(\varepsilon) - T_e^*]\}$$

$$\phi(\varepsilon) = \frac{T_1^*(\varepsilon)[\delta^* + (1-2\varepsilon)\tan\alpha]}{[\delta^* + (1-N_R)\tan\alpha]} + (N_R - \varepsilon)\psi(\varepsilon)$$

The constant C is given in eq. (18c) with $\zeta_1 = 1$.

The advantages of the integral formulation in eq. (19) over the differential equation in eq. (18a) are: (1) the boundary conditions are included in the equation and (2) the equation is in the same form as the radiation equations, a form which readily lends itself to an iterative type solution. Specific details regarding the solution of eqs. (16), (17) and (19) for the distributions of $Q_1(\zeta_1)$, $Q_b(\tau_b)$ and $T_1^*(\zeta_1)$ are given in Appendix B.

Total Heat Transfer and Fin System Effectiveness. The heat transfer rate from the finned tube section between the two vertical center-lines in Figure 2 is equal to the sum of the radiative and convective contributions. The radiative contribution, q_R, is

$$q_R = 2 \int_{R_i}^{R_o} q_1(r_1)\, 2\pi r_1 \frac{dr_1}{\cos\alpha} + \int_{(R_o - R_i)\tan\alpha}^{L - (R_o - R_i)\tan\alpha} q_b(z_b)\, 2\pi R_i\, dz_b$$
$$+ 2\,(2\pi R_o \delta)[\varepsilon\sigma(T_1^4(R_o) - T_e^4)] \qquad (20)$$

The integrand under the first integral in eq. (20) is the product of the local radiative flux, $q_1(r_1)$, and the area of the ring element, dA_1, in Figure 3. Integrating over the entire fin surface area and multiplying the result by the factor 2 to take into account the contribution the opposite fin surface A_2 gives the net radiative loss from the two conical surfaces. The second integral gives the net radiative loss from the base surface between the fins. The last term represents the radiative loss from the two fin tips of area $(2\pi R_o \delta)$ at temperature $T_1(R_o)$.

The convective loss, q_c, is written similarly as

$$q_c = 2 \int_{R_i}^{R_o} h(T_1(r_1) - T_e) \frac{2\pi r_1 dr_1}{\cos \alpha} + (2\pi R_i)(L-2(R_o-R_i)\tan\alpha)h(T_b-T_e) + 2(2\pi R_o \delta)h(T_1(R_o)-T_e) \quad (21)$$

where the second term represents the convective loss from the isothermal tube surface.

A common method of assessing the enhancement in total heat transfer rate, q_T, due to the addition of fins is to compare this value with the rate of heat transfer from the unfinned cylinder, q_o. The latter quantity is given by

$$q_o = 2\pi R_i (L+2\delta)[\varepsilon\sigma(T_b^4 - T_c^4) + h(T_b - T_e)] \quad (22)$$

The comparative index is called the "fin system effectiveness" by Donovan [8] and is written as

$$\eta = \frac{q_T}{q_o} = \frac{q_R + q_c}{q_o} \quad (23)$$

Fins are effective in increasing the heat transfer rate when the fin configuration and thermal properties are such as to produce values of $\mathfrak{z}$ greater than unity. From the manufacturing point of view, $\mathfrak{z}$ should be substantially above unity. Systems with $\mathfrak{z}$ less than unity must be avoided because, in this case, the fins have an insulating effect on the base tube.

In dimensionless form the fin system effectiveness is given by

$$\mathfrak{z} = \frac{N_c Q_R + h^* Q_c}{Q_o} \tag{24}$$

where

$$Q_R = 2\int_{N_R}^{1} Q_1(\zeta_1)\frac{\zeta_1 d\zeta_1}{\cos\alpha} + N_R\int_{(1-N_R)\tan\alpha}^{N_L-(1-N_R)\tan\alpha} Q_b(\tau_b)d\tau_b + 2\delta^*\varepsilon[T_1^{*4}(1)-T_e^{*4}]$$

$$Q_c = 2\int_{N_R}^{1}(T_1^*(\zeta_1)-T_e^*)\frac{\zeta_1 d\zeta_1}{\cos\alpha} + N_R(1-T_e^*)[N_L-2(1-N_R)\tan\alpha] + 2\delta^*[T_1^*(1)-T_e^*]$$

$$Q_o = N_R(N_L + 2\delta^*)[\varepsilon N_c(1-T_e^{*4}) + h^*(1-T_e^*)]$$

The computer program listed in Appendix C calculates the distributions of $Q_1(\zeta_1)$, $Q_b(\tau_b)$ and $T_1^*(\zeta_1)$. Through the above equations it then computes $\mathfrak{z}$. With a little algebra it can be shown that the actual heat transfer rate is related to $\mathfrak{z}$ and Q_o by the expression

$$q_T = (2\pi\mathfrak{z}Q_o/N_R^2)(R_o T_b k_m \cos\alpha)(\delta^* + (1-N_R)\tan\alpha) \tag{25}$$

APPLICATION OF THEORY TO THE DESIGN OF A MORTAR TUBE

Input Data. As an application of the theory the heat transfer characteristics of the fin configuration used on the XM144E1 mortar tube (see Figure 1) were calculated. The ambient air temperature, T_e, was taken as 100°F in all of the calculations. The emissivity, ϵ, the metal thermal conductivity, k_m, and the tube temperature, T_b, were varied as shown in Table I below.

Table I

ϵ = 0.75, 1.0

k_m = 10, 25 Btu/hr-ft-°F

T_b = 800°F - 1200°F

The emissivity values are typical of the coatings used on mortars operating in this temperature range. The low value of k_m is typical of a high nickel content alloy while the higher value corresponds to a higher iron content.

The three parameters -- ϵ, k_m and T_b -- are characteristics of a particular material; the maximum allowable tube temperature is related to the mechanical properties of the tube. It is clear before any results are presented that the material with the highest values of this set of parameters will give the highest heat transfer rate -- the present calculations are intended to show the relative importance of each of the parameters. The effect of changes in geometry for given ϵ, k_m and T_b will be considered in a later section.

Calculation of the Dimensionless Convection Coefficient, h*. The dimensionless convection coefficient, h*, can be put in the form

$$h^* = \left(\frac{hL}{k_a}\right)\left(\frac{k_a}{k_m}\right) \quad \frac{K_i^2}{L\cos\alpha[\delta + (R_o - R_i)\tan\alpha]}$$

where the product (Lk_a) has been introduced in the numerator and denominator (k_a is the thermal conductivity of the air and L is defined in Figure 2). The dimensionless grouping (hL/k_a) is recognized as the Nusselt number.

Correlations for free convection heat transfer from finned tubes are given by Knudsen and Pan [9] and Nwizu [10]. Both correlations are restricted to straight ($\alpha = 0$), isothermal ($T_f(r_f) = T_b$) fins on a horizontal cylinder. In addition, their tests were limited to tubes with diameters of 1-1/2" or less and a maximum temperature of 350°F. Although the short fins shown in Figure 1 do operate in a nearly isothermal condition the limitations on surface temperature and particularly tube orientation raise considerable doubt as to the applicability of their work to mortar operating conditions. The geometric limitations also introduce some uncertainty. Thus, while these correlations should not be applied in an actual mortar design situation they do serve the purpose here of relating the convection coefficient to the temperature dependent air properties and to the fin geometry. The need for further experimental work in this area is evident.

Over the range of variables of interest here Nwizu's correlation can be written as

$$\frac{hL}{k_a} = 0.058\left[\frac{g\beta\rho^2}{\mu^2} L^3 \quad (T_b - T_e)\right]^{0.45} \tag{26}$$

where β is the coefficient of thermal expansion (1/°F), ρ is the density (lb_m/ft^3), g is the acceleration due to gravity (32.2 ft/sec^2) and μ is the viscosity (lb_m/ft-sec.). All air properties are evaluated at the temperature $(T_b + T_e)/2$.

Heat Transfer Results. The results of the above calculation are presented in Figures 4 and 5. Of the two sets of curves plotted in Figure 4 the upper set represents the total heat transfer per unit tube length; that is,

$$\bar{q}_T = \frac{q_T}{S} = \frac{q_R + q_C}{S} \tag{27}$$

where q_R and q_C are, respectfully, the radiative and convective portions of the total heat transfer (see eqs. (20) and (21)) from the fin-tube section of axial length $S = L + 2\delta$ (see Figure 2). The lower set of curves in Figure 4 represents the radiative contribution alone where $\bar{q}_R = q_R/S$.

Of the three parameters shown in the figure the base temperature, T_b, has the dominant effect on the heat transfer. This is primarily due to the tremendous increase in radiative transfer with temperature. Consider the uppermost curve in each set, that is, $\epsilon = 1.0$ and $k_m = 25$ Btu/hr-ft-°F. At $T_b = 800$ °F radiation accounts for roughly 56% of the total heat transfer. Increasing the base temperature to 1200 °F more than doubles $\bar{q}_T$ and, at this temperature, radiation accounts for over 70% of the total.

These results can be explained by noting that the potential for convective transfer is $(T_b - T_e)$ while that for radiative transfer is $(T_b^4 - T_e^4)$. Increasing T_b from 800 °F (1260 °R) to 1200 °F (1660 °R) while keeping T_e = 100 °F(560 °R) increases the temperature potentials for convective and radiative transfer by roughly 57% and 208%, respectfully. The actual calculations show a 53% increase in convection and a 200% increase in radiation; the discrepancy is due to the temperature drop along the fin which reduces the average potentials for heat transfer somewhat. The magnitude of the radiative contribution indicated in Figure 4 justifies the tedious calculations required to obtain it.

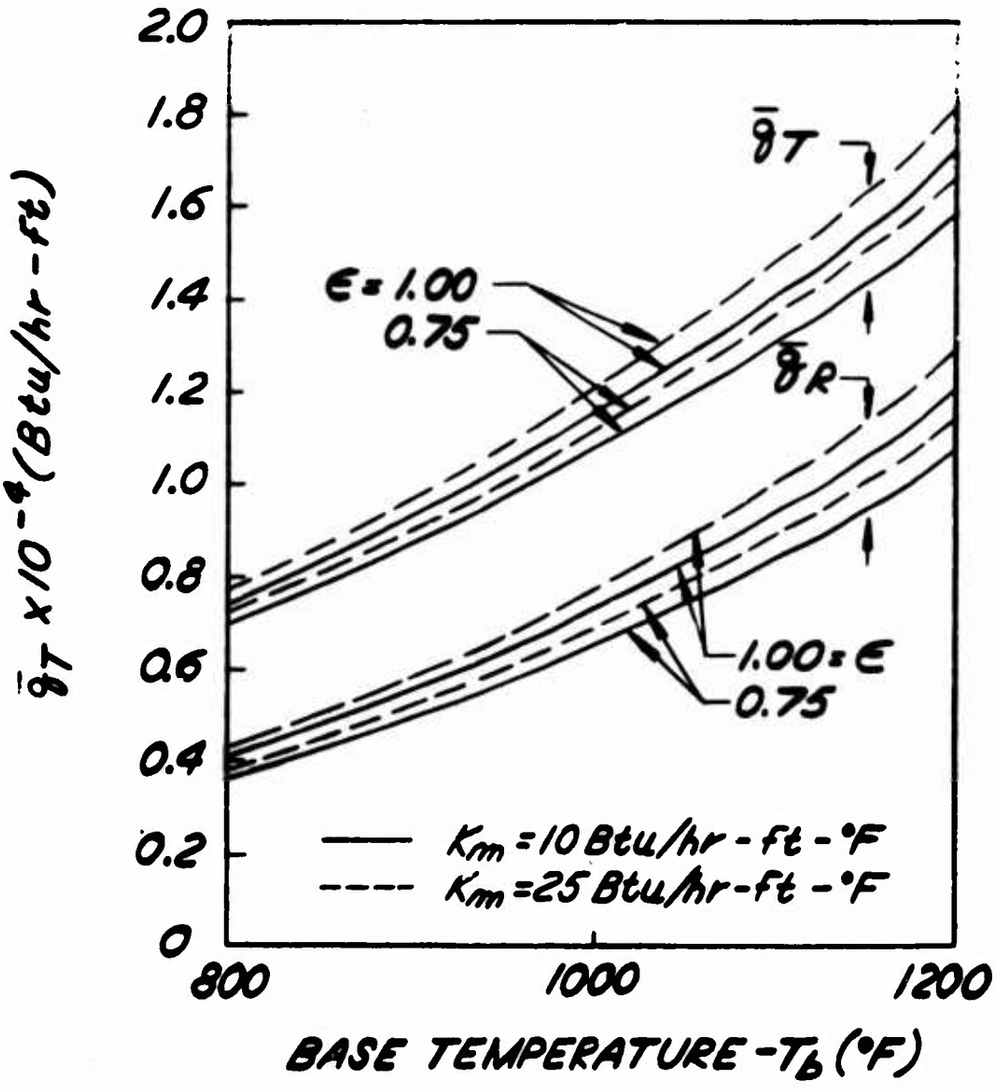

FIGURE 4. HEAT TRANSFER RESULTS FOR THE GEOMETRY SHOWN IN FIGURE 1.

Reducing the surface emissivity from unity to $\varepsilon = 0.75$, a 25% decrease, reduces the radiative transfer by only about half this amount. This surprising result is explained by the so called "cavity effect". When ε is unity the only radiation which escapes from the fin-tube cavity is that which is emitted by a warm surface in the direction of the fictitious cold surface "e" in Figure 2. All other radiation is completely absorbed by the remaining black surfaces of the enclosure. Decreasing the emissivity decreases the emissive power of each elemental area in the enclosure but at the same time it increases the probability of escape of radiation from the enclosure by the process of multiple reflections. Thus, radiation emitted by one warm element in the direction of a second warm element may be reflected by the latter surface in the direction of surface "e" and escape from the system. The net result is a decrease in net radiative loss from the enclosure which is substantially less than the decrease in emissivity. The converse, of course, is also true -- increasing the emissivity does not result in a proportionate increase in radiative transfer. Therefore, if a particular coating is found to be satisfactory from the viewpoint of durability and has an emissivity of 0.8-0.9 at the desired operating temperature, very little will be gained by searching for a coating with a higher emissivity.

The thermal conductivity of the fin material, k_m, is seen to have a very small effect on the overall heat dissipation rate in Figure 4. This is far from the general state of affairs, however, as will be seen later when the effect of geometry is considered. For the short fins under consideration here, most of the resistance to heat transfer is encountered at the fin surface. The temperature drop along the fin amounts to only a few percent for all of the cases in Figure 4.

Fin System Effectiveness. The fin system effectiveness, $\mathfrak{z}$, was defined earlier as the ratio of the heat transfer rates from the finned and smooth cylinders, respectfully, or

$$\mathfrak{z} = \frac{q_T}{q_o} = \frac{\bar{q}_T}{\bar{q}_o} \tag{28}$$

A plot of $\mathfrak{z}$ is shown in Figure 5 for the fin system under consideration. The decrease in $\mathfrak{z}$ with increasing base temperature results from the fact that the radiative and convective contributions to $\bar{q}_o$ increase exactly in proportion to the potentials $(T_b^4 - T_e^4)$ and $(T_b - T_e)$, respectfully, whereas, as noted earlier in the discussion of Figure 4, the average temperature potentials in the calculation of $\bar{q}_1$ are somewhat lower due to thermal resistance within the fin. Thus, the ratio in eq. (28) is a decreasing function of temperature and the fin system becomes less effective at higher temperatures.

Increasing the thermal conductivity, k_m, produces a relatively small increase in $\mathfrak{z}$. The increase is due to the fact that energy is more easily transported to the outer regions of the fin resulting in higher average temperature levels and a more effective utilization of the entire fin. In very tall fins or with poor conductors the thermal conductivity can have a much more pronounced effect on $\mathfrak{z}$.

The surface emissivity, ε, has a strong effect on $\mathfrak{z}$. Decreasing ε by 25% decreases the radiative contribution of the smooth cylinder by the same amount but, due to the cavity effect noted earlier, the decrease in the finned tube heat transfer rate is only about half this amount. Therefore, the ratio in eq. (28) increases with decreasing ε. Thus, the addition of

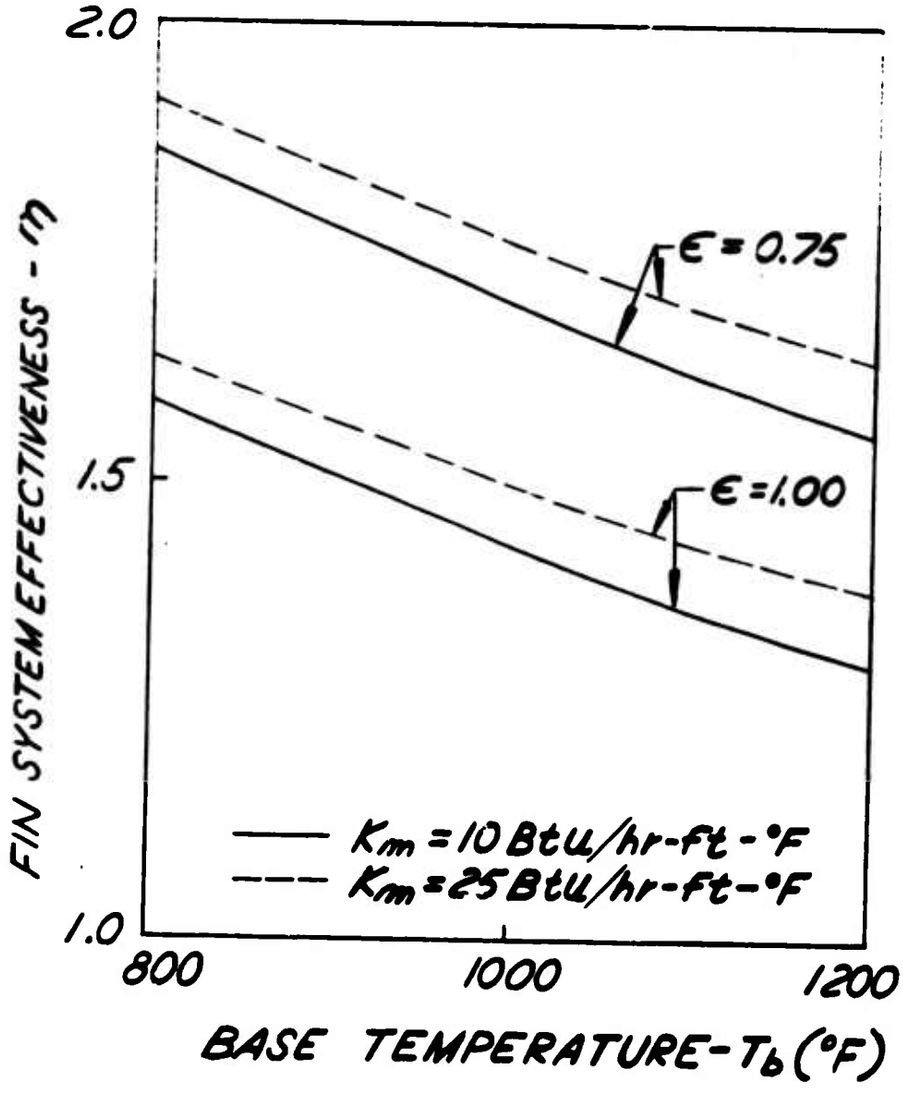

FIGURE 5. FIN SYSTEM EFFECTIVENESS FOR THE GEOMETRY SHOWN IN FIGURE 1.

fins is more effective in augmenting heat transfer in systems with low emissivity.

With regard to the mortar tube configuration shown in Figure 1 the results in Figure 5 indicate that the addition of fins represents an augmentation in heat transfer on the order of 50%, assuming a relatively high emissivity. This increase, while significant, still leaves a wide gap between the maximum permissible firing rate and the desired rate; that is, the rate at which an individual can load the weapon. Assuming a material has been chosen, that is, assuming ϵ, k_m and T_b have been specified, the only recourse left to the designer is to alter the fin geometry. This will now be considered.

Alternate Fin Configurations. In general, the designer must stay within a certain weight limitation in choosing alternate fin configurations. The weight, or equivalently, the volume of metal per unit length which the fins contribute is

$$\bar{V} = \left(\frac{4\pi}{S}\right)\left[\delta(R_o^2-R_i^2) + \frac{\tan\alpha}{3}(R_o-R_i)(R_o^2+R_iR_o-2R_i^2)\right] \qquad (29)$$

In the present set of calculations $\bar{V}$ was kept constant and equal to $\bar{V}_o$ which was calculated for the fin configuration shown in Figure 1; that is, all of the alternate designs considered here have the same weight per unit length. In addition, the fin tip thickness, δ, and the tube radius, R_i, were also fixed at the values shown in Figure 1. The fin spacing S was given the values $S_o/2$, S_o, $3S_o/2$ and $2S_o$ where S_o is the fin spacing in Figure 1. The angle α was taken as 0°, 2°, 4°, 6° and 8°. The remaining variable, R_o, was calculated from eq. (29) with $\bar{V} = \bar{V}_o$. The resulting twenty configurations are shown in Figures 6a - 6d.

$s = 0.5 s_0 = 0.125$
$\delta = 0.015$

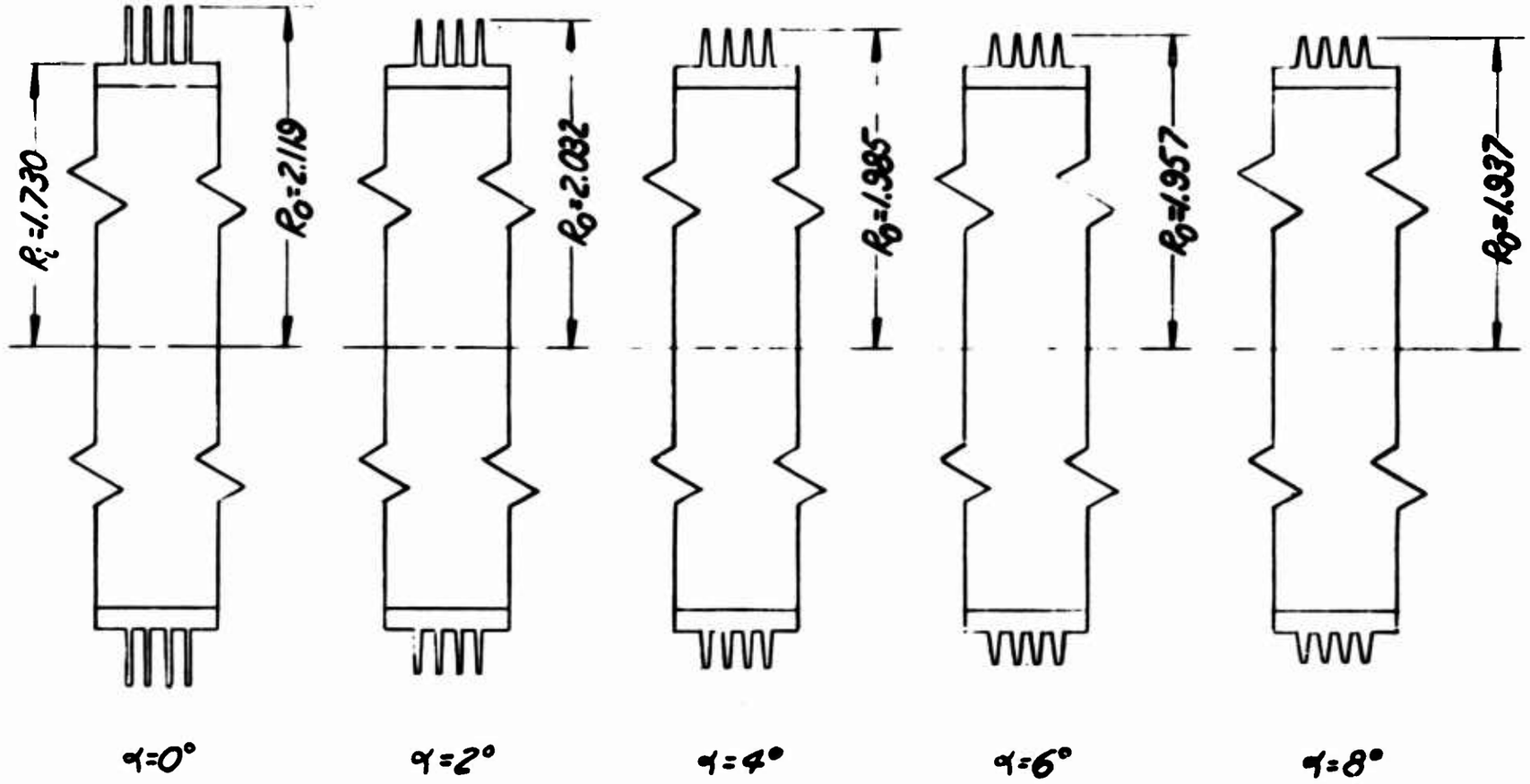

FIGURE 6a . FIN CONFIGURATIONS WITH $s = s_0/2$.

$s = s_0 = 0.250$
$\delta = 0.015$

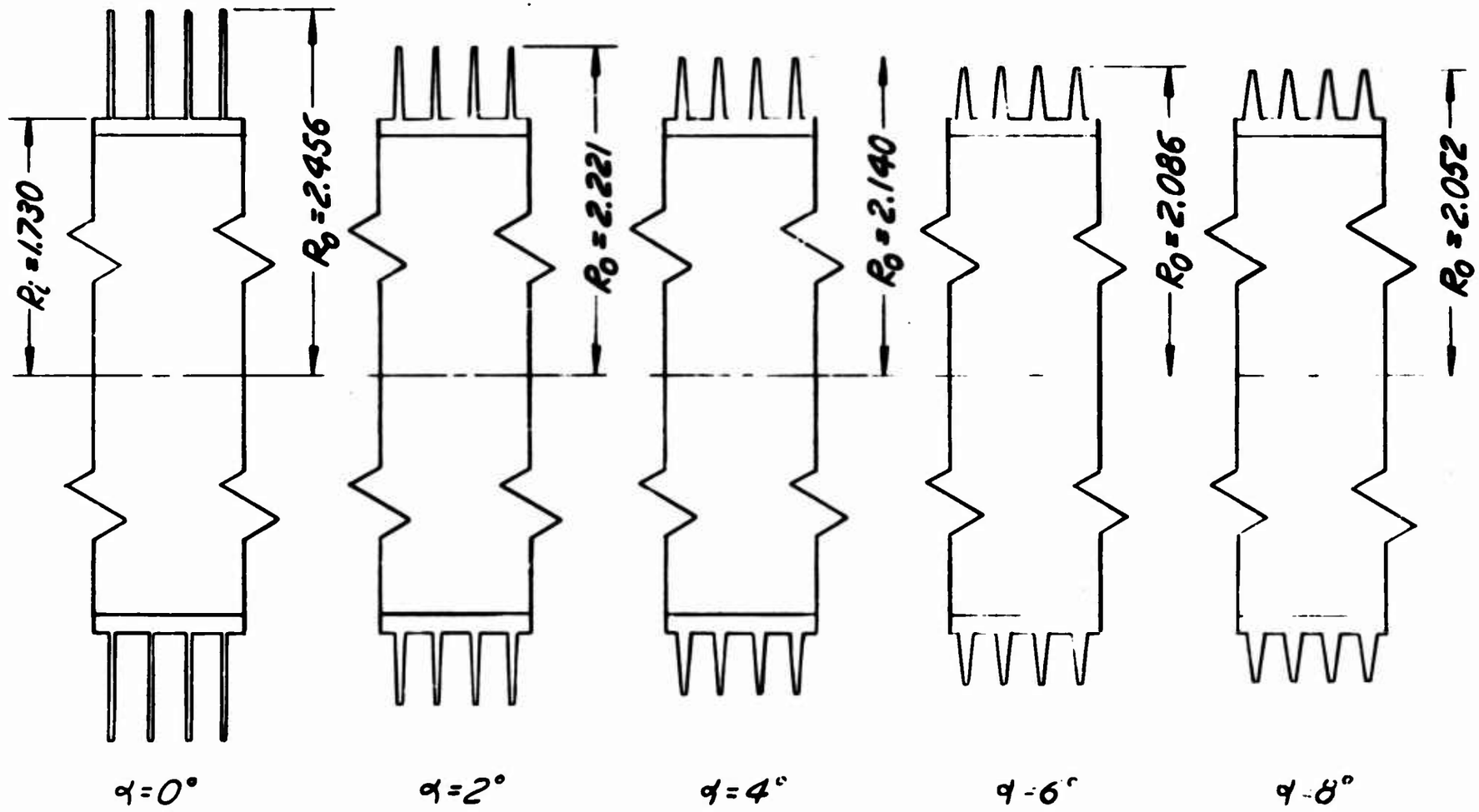

FIGURE 66. FIN CONFIGURATIONS WITH $s = s_0$.

$s = 1.5 s_o = 0.375$

$\delta = 0.015$

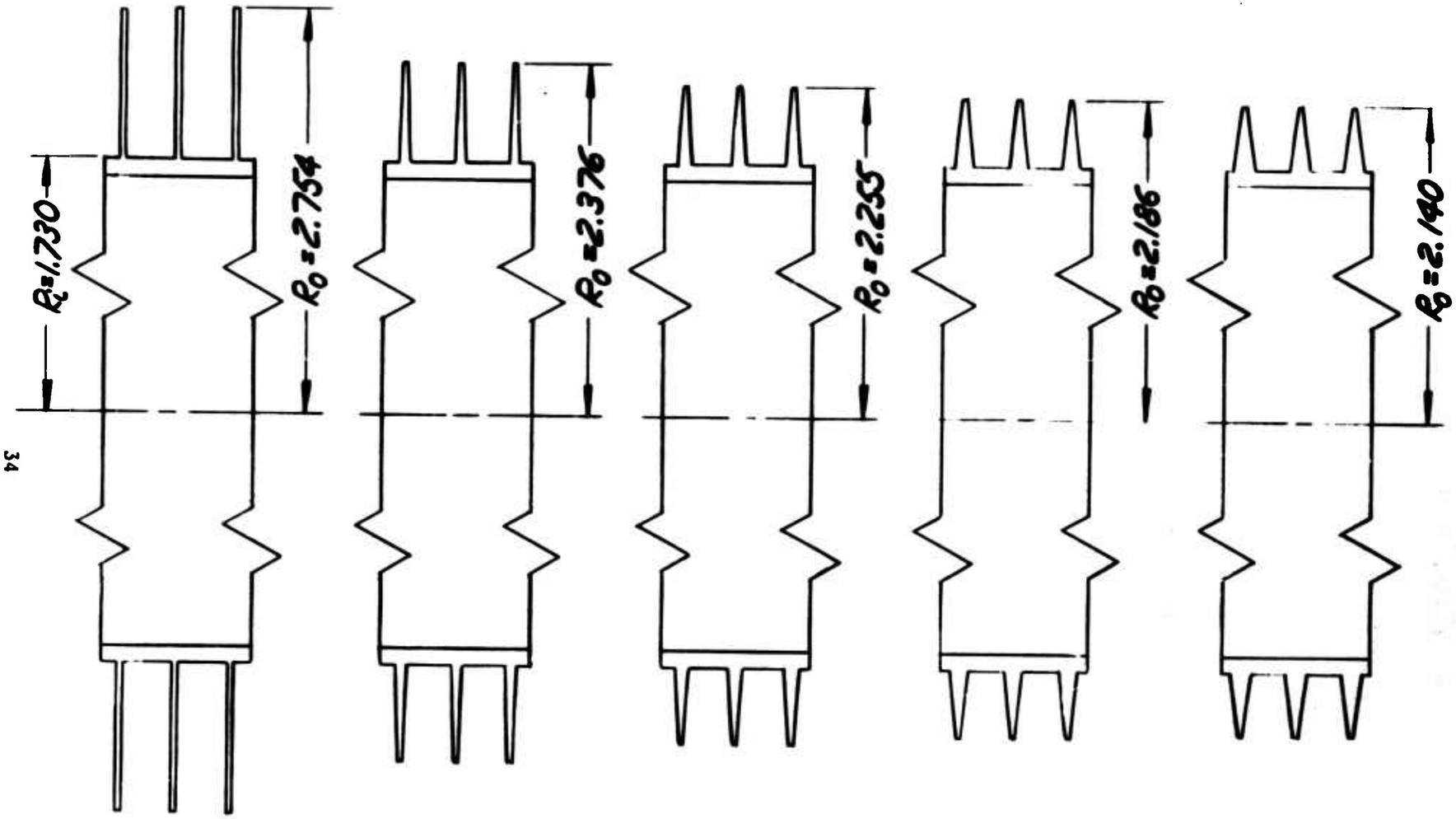

FIGURE 6c. FIN CONFIGURATIONS WITH $s = 3s_o/2$.

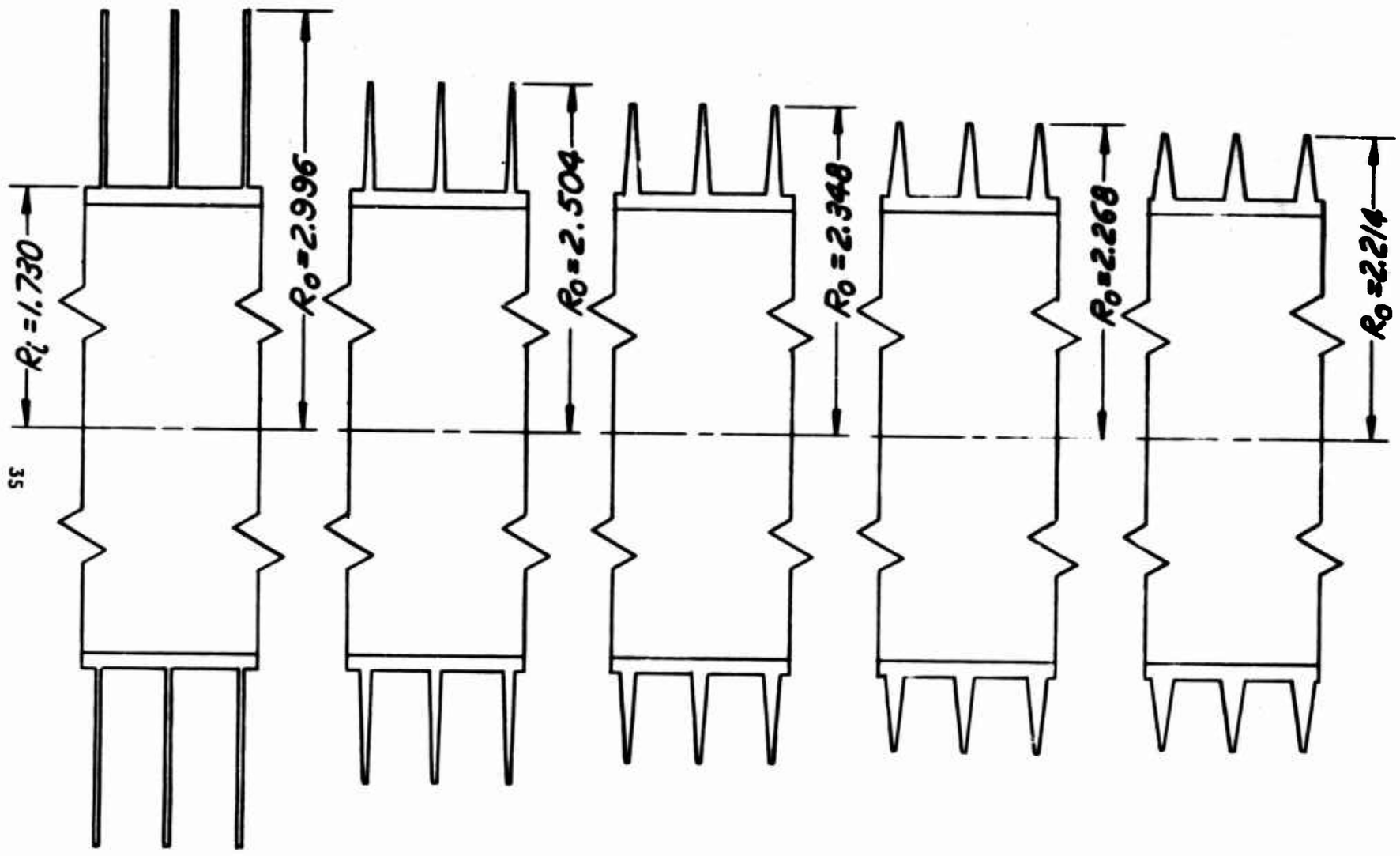

FIGURE 6d. FIN CONFIGURATIONS WITH $S = 2 S_0$.

It is noted in the figures that for a given fin spacing, S, decreasing α results in taller fins and a greater surface area per unit tube length. Increasing the fin spacing for a given α also increases the fin height but the surface area per unit length does not change appreciably because the number of fins per unit length decreases with increasing S.

Effect of Geometry on Heat Transfer. The total heat transfer rate per unit length, $\bar{q}_T$, was evaluated at eight sets of the parameters ϵ, k_m and T_b for each of the twenty configurations shown in Figures 6a-6d. The results are presented in Figures 7a-7h. Each figure gives the results for one set of ϵ, k_m and T_b.

Consider Figure 7a. Each point on the curved surface represents the percentage change in $\bar{q}_T$ for that geometry (S and α) relative to $\bar{q}_T$ for the XM144E1 fin configuration shown in Figure 1 at the values of ϵ, k_m and T_b listed at the top of the figure. The value of $\bar{q}_T$ given in the figure title corresponds to the XM144E1 fin configuration. Thus, the fin configuration with $\alpha = 0°$ and $S = 2S_o$ (see Figure 6d for this geometry) dissipates approximately 10% more heat than the XM144E1 mortar or $\bar{q}_T = 1.1 \times 0.870 \times 10^4$ Btu/hr-ft $= 0.957 \times 10^4$ Btu/hr-ft. When $\alpha = 8°$ and $S = S_o/2$ (see Figure 6a) the heat transfer rate is roughly 7% below that for the XM144E1 mortar configuration. Seventeen of the twenty configurations in Figures 6a-6d are seen to dissipate more heat than the configuration shown in Figure 1.

Comparing Figures 7a and 7b shows that increasing the emissivity causes a general flattening of the surface although the reduction is not large. The same effect is noted in the other three pairs of figures when the emissivity is the only parameter changed. The increase in ϵ increases the emissive power of each elemental area of the fin surfaces which, in turn,

increases the temperature drop along the fin to balance the energy demand. This results in a less effective utilization of the outer portions of the fin and the effect is most apparent in the taller fins ($\alpha = 0°$). Increasing the temperature level also increases the radiative transfer and has the same effect on the shape of the surface as ϵ. Compare Figures 7a and 7c or Figures 7b and 7d, for example.

Increasing the thermal conductivity, k_m, markedly improves the heat transfer because of the more efficient transport of energy to the outer portions of the fins. The effect is strongest as the fin height increases (decreasing α). Compare Figures 7a - 7d with Figures 7e - 7h respectively.

When the fin spacing is small ($S = S_o/2$), decreasing α increases the heat transfer because of the increase in fin surface area. At large fin spacings ($S = 2S_o$) the heat transfer rate at first increases with decreasing α, reaches a maximum and then may decrease slightly, as in Figures 7a - 7d. The decrease can be attributed to the difficulty in transporting energy to the outer portions of the taller fins ($\alpha = 0°$) when the fin thermal conductivity is low.

Concluding Remarks. Once a material is chosen, that is, after the parameters ϵ, k_m and T_b are specified, a surface such as those in Figures 7a - 7h can be constructed. The problem is then to choose the highest point on the surface consistent with the structural integrity of the tube. The importance of being able to predict tube strength for an arbitrary fin configuration is apparent.

All of the surfaces seem to have a maximum in the interval $S_o/2 < S < S_o$; that is, the analysis seems to favor small fin spacings. This conclusion

FIGURE 7a. CHANGE IN HEAT TRANSFER WHEN $T_b = 900°F$, $K_m = 10$ Btu/hr-ft-°F, $\epsilon = 0.75$ AND $\bar{q}_T = 0.870 \times 10^4$ Btu/hr-ft.

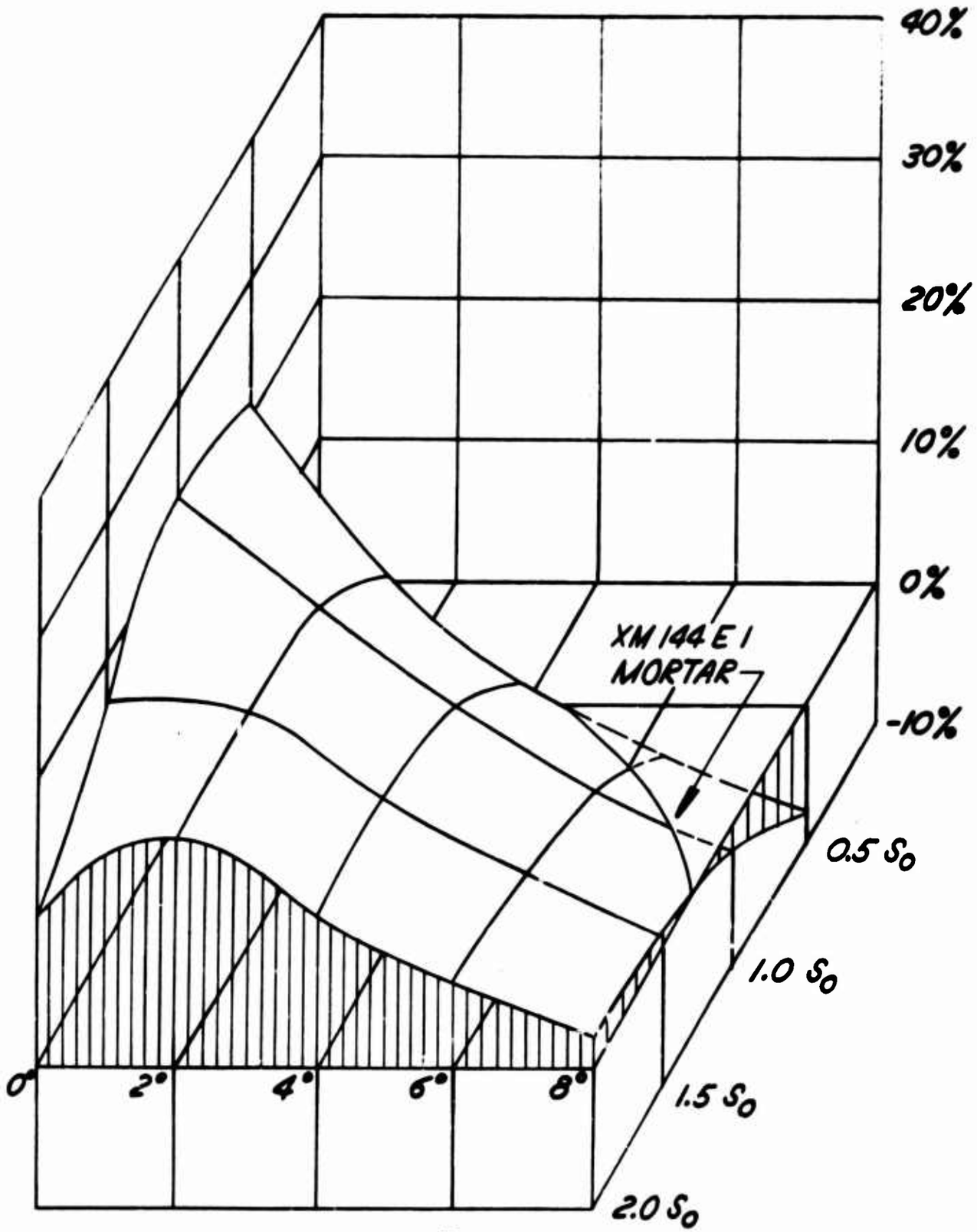

FIGURE 7b. CHANGE IN HEAT TRANSFER WHEN $T_b = 900°F$, $K_m = 10$ Btu/hr-ft-°F, $\epsilon = 1.0$ AND $\bar{q}_T = 0.931 \times 10^4$ Btu/hr-ft.

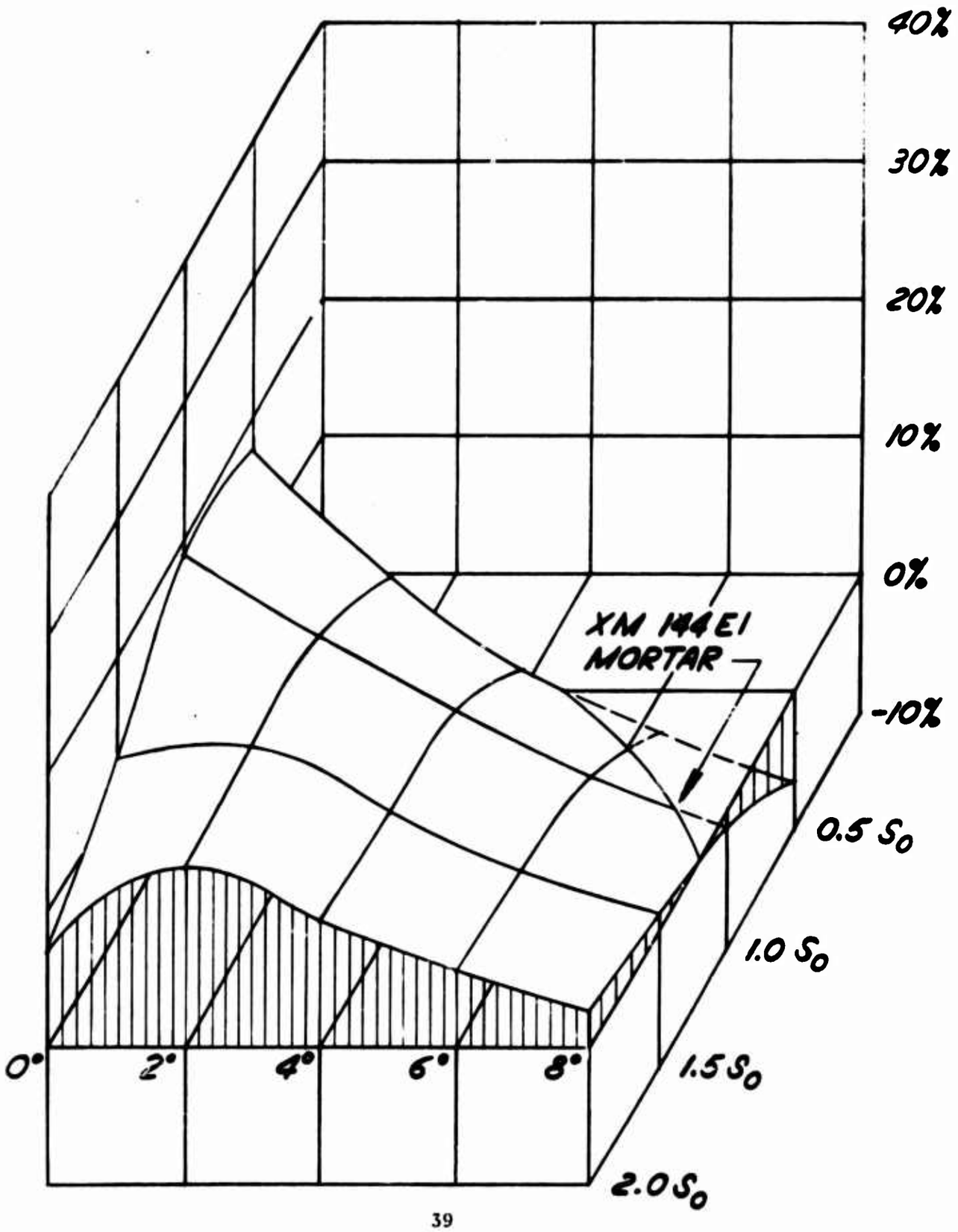

FIGURE 7c. CHANGE IN HEAT TRANSFER WHEN $T_b = 1100°F$, $k_m = 10$ Btu/hr-ft-°F, $\epsilon = 0.75$ AND $\bar{q}_T = 1.311 \times 10^4$ Btu/hr-ft.

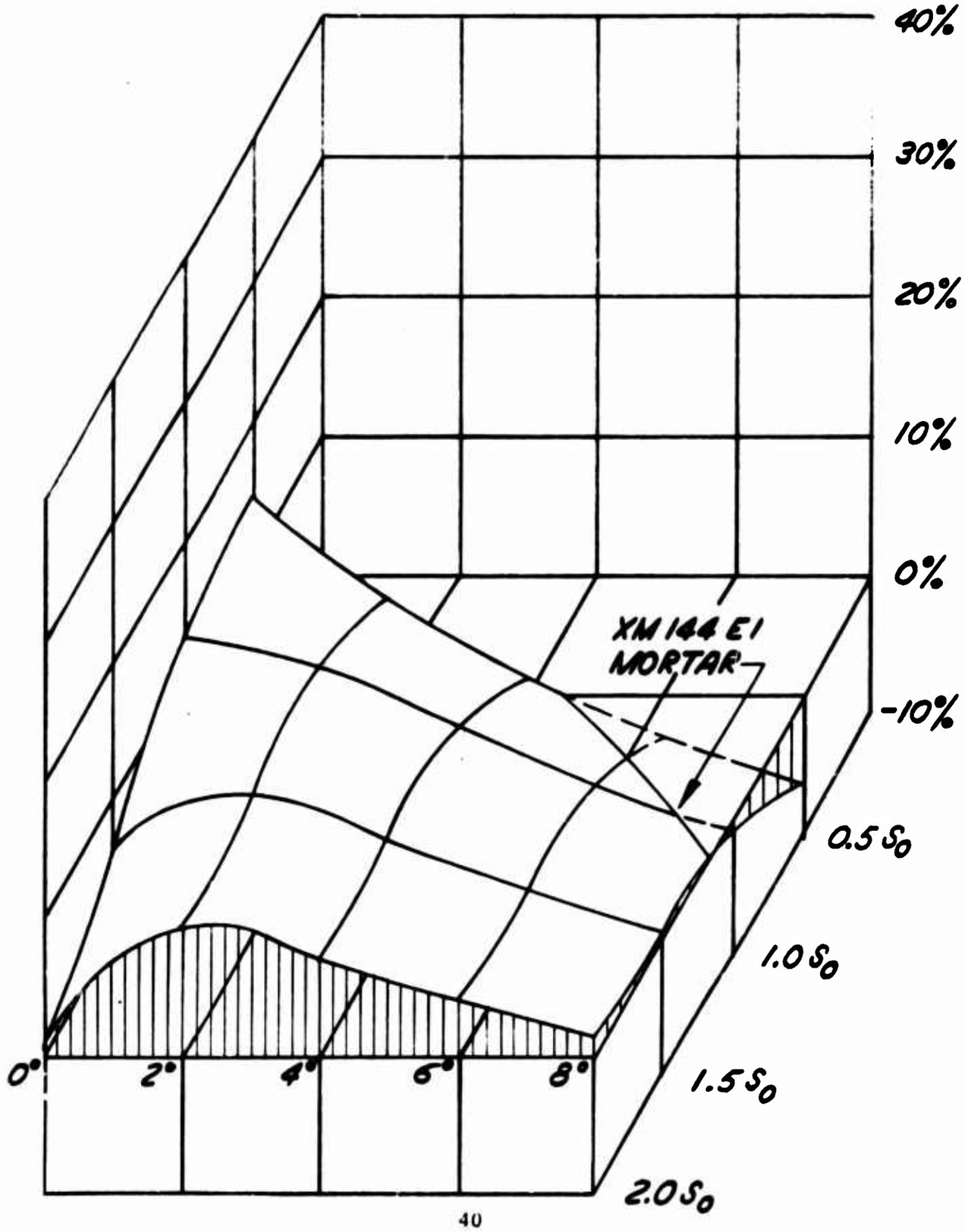

might be altered somewhat if the orientation of the mortar tube with respect to the horizontal could be taken into account in the calculation of the convection coefficient. Wider fin spacings that offered less impedance to the vertical air flow would probably be favored. Since the large radiative contribution is independent of the tube orientation the results are probably not significantly in error, however.

Finally, it should be emphasized that all of the heat transfer results are based on one tube weight per unit length, one fin tip thickness, δ, one tube radius, R_i, and it was assumed that the fin material had a conductivity on the order of that for steel or steel alloys -- as opposed to a better conductor such as aluminum. Thus, this study should be viewed more as a qualitative analysis or method of interpretation of the type of results which can be obtained with the computer program in Appendix C rather than a quantitative recommendation for future mortar designs.

FIGURE 7d. CHANGE IN HEAT TRANSFER WHEN $T_b = 1100°F$, $k_m = 10$ Btu/hr-ft-°F, $\epsilon = 1.0$ AND $\bar{q}_T = 1.411 \times 10^4$ Btu/hr-ft.

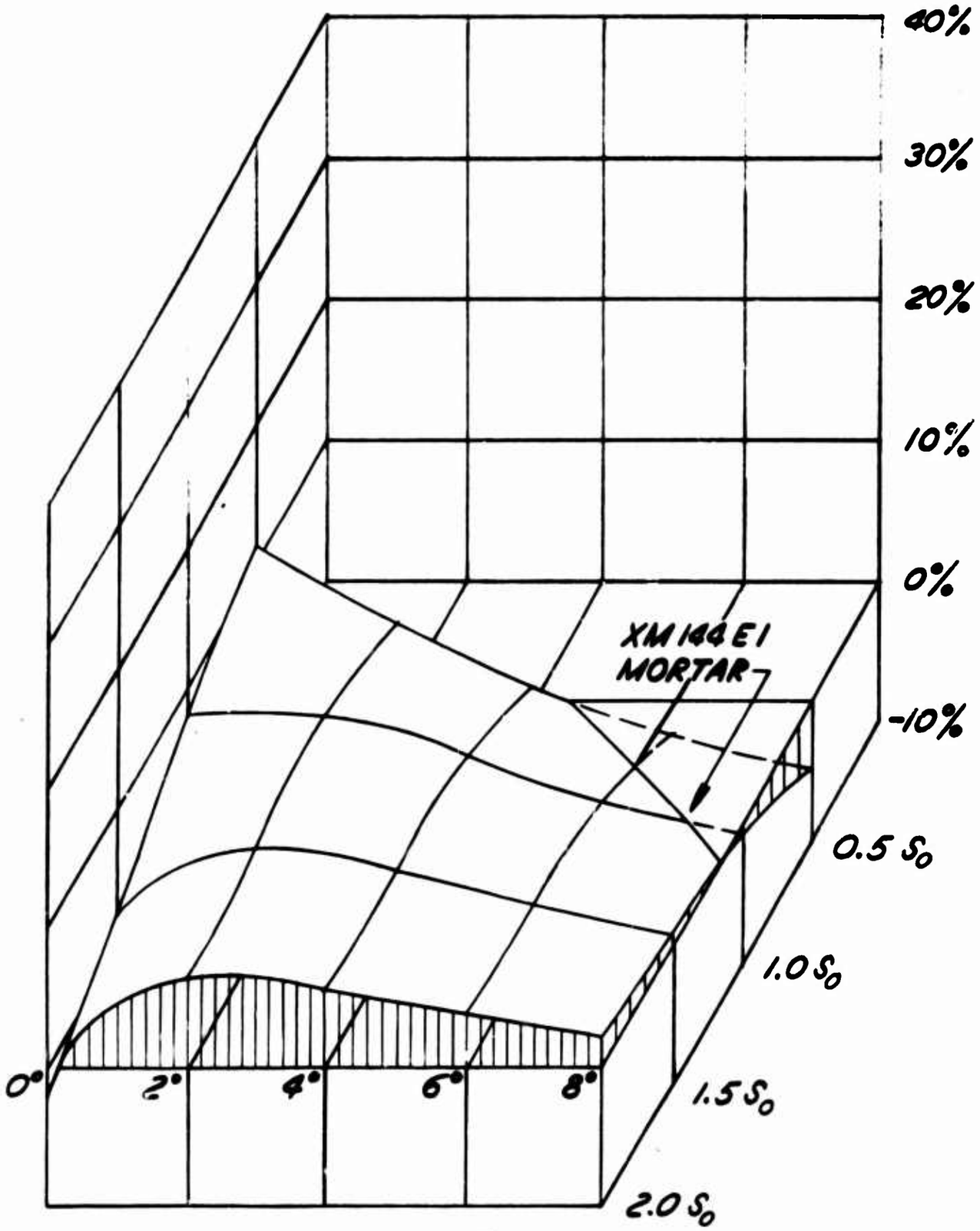

FIGURE 7e. CHANGE IN HEAT TRANSFER WHEN $T_b = 900°F$, $K_m = 25$ Btu/hr-ft-°F, $\epsilon = 0.75$ AND $\bar{q}_T = 0.899 \times 10^4$ Btu/hr-ft.

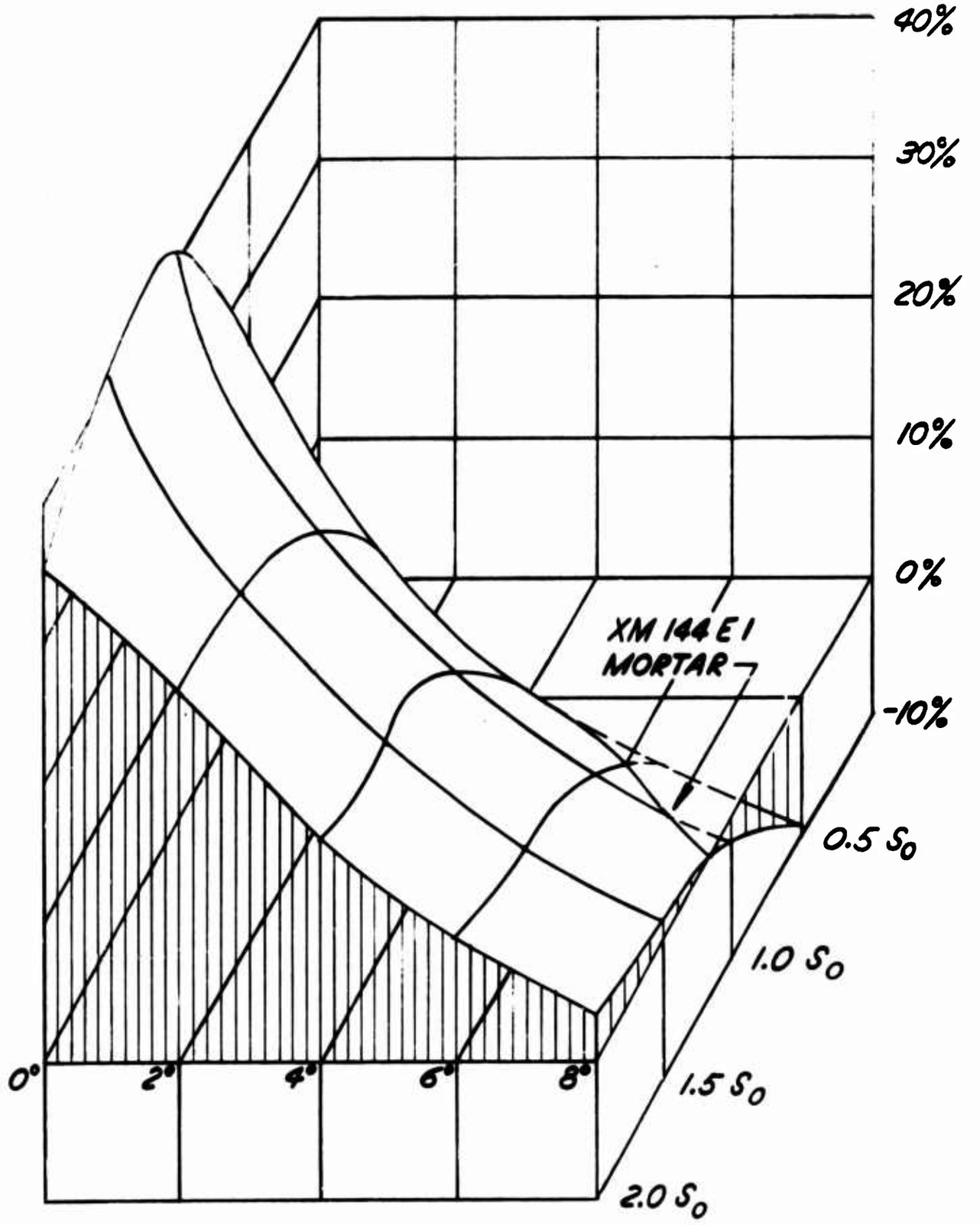

FIGURE 7f. CHANGE IN HEAT TRANSFER WHEN $T_b = 900°F$, $K_m = 25$ Btu/hr-ft-°F, $\epsilon = 1.0$ AND $\bar{q}_T = 0.966 \times 10^4$ Btu/hr-ft.

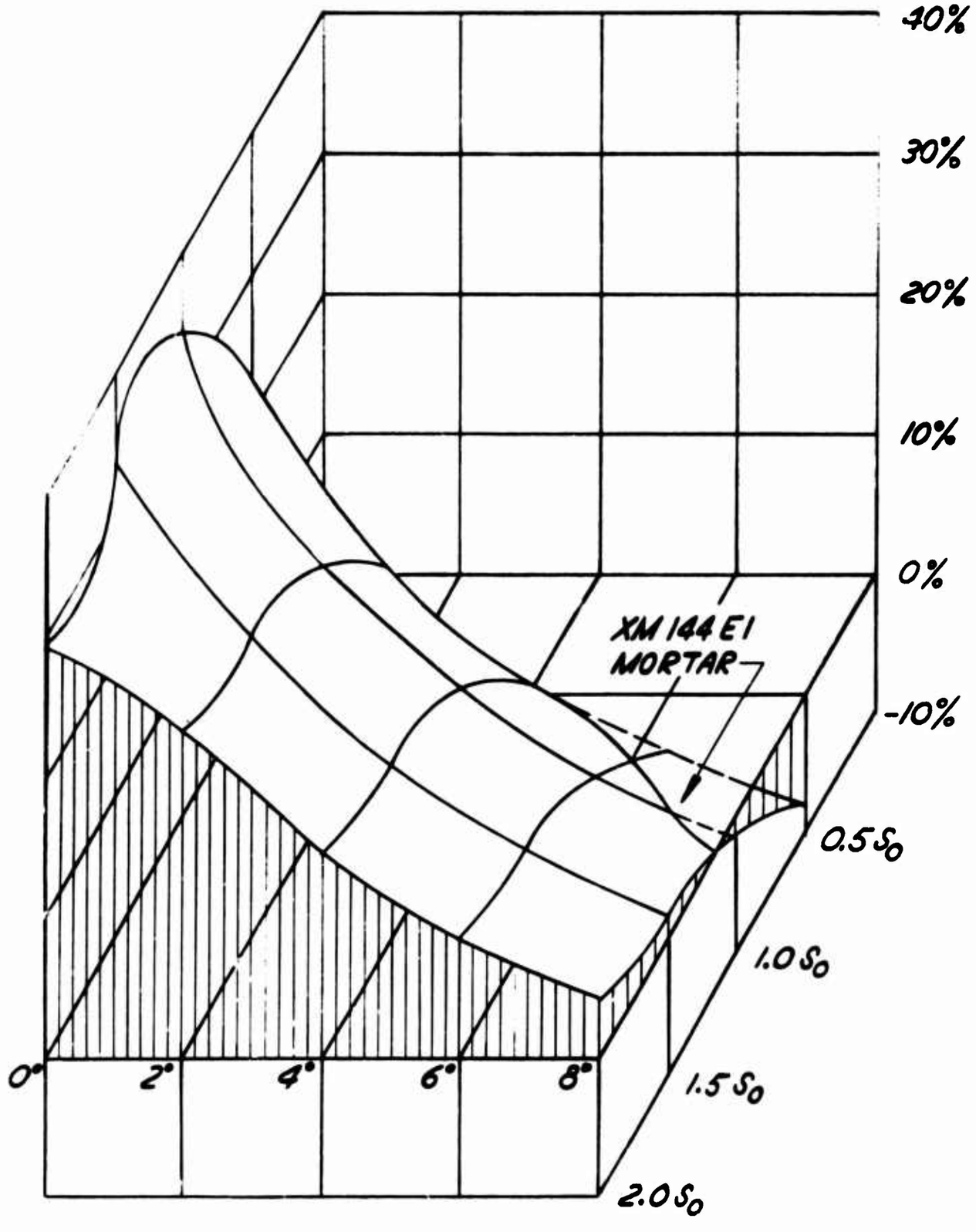

FIGURE 7g. CHANGE IN HEAT TRANSFER WHEN $T_b = 1100°F$, $k_m = 25$ Btu/hr-ft-°F, $\epsilon = 0.75$ AND $\bar{q}_T = 1.370 \times 10^4$ Btu/hr-ft.

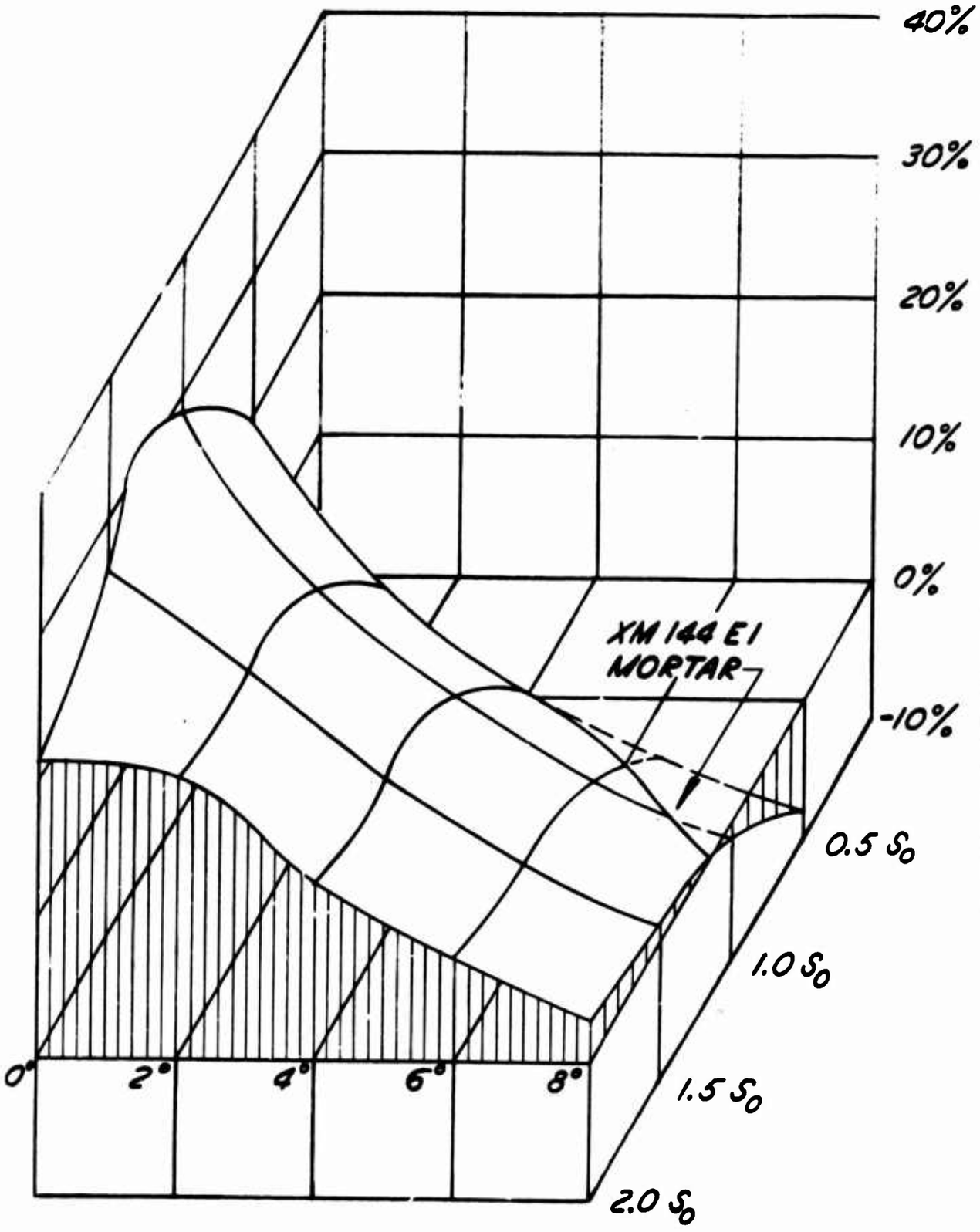

FIGUPE 7h. CHANGE IN HEAT TRANSFER WHEN $T_b = 1100°F$, $k_m = 25$ Btu/hr-ft-°F, $\epsilon = 1.0$ AND $\bar{q}_T = 1.484 \times 10^4$ Btu/hr-ft.

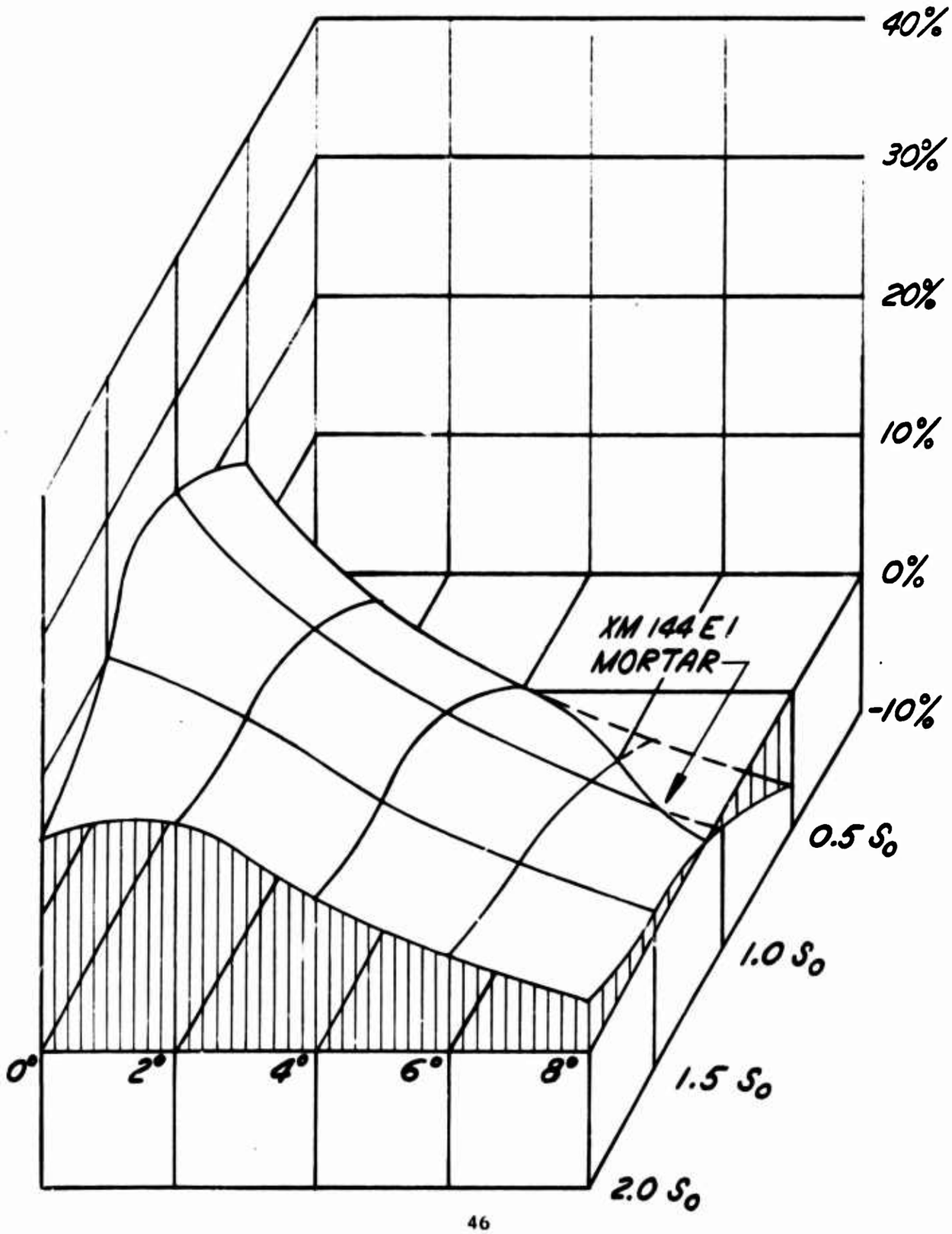

CONCLUSIONS AND RECOMMENDATIONS

A method is demonstrated for calculating the steady heat transfer rate from finned cylinders dissipating energy to the surroundings by convection and radiation. Application of the method to the XM144E1 mortar revealed that the radiative mode accounts for 60-70% of the total energy transfer under some operating conditions. Lack of adequate convective heat transfer data under these conditions renders the calculations somewhat tentative, however, and it is recommended that more precise experimental data be obtained in this area.

It was also found that changing the fin configuration on the XM144E1 mortar, while maintaining the same weight per unit tube length, can further augment the heat transfer rate. Strength considerations can limit the gains achieved through changes in geometry, however, so it is further recommended that appropriate experimental data be acquired, probably by photoelastic methods, for predicting the load carrying characteristics of arbitrary fin configurations. This data can then be used as a guide in the selection of the optimum fin configuration -- optimum from the viewpoint of heat transfer.

REFERENCES

1. Kraus, A.D., Extended Surfaces, Spartan Books, Inc., Baltimore, Md. (1964).

2. Sparrow, E.M., G.B.Miller and V.K.Jonsson, "Radiating Effectiveness of Annular-Finned Space Radiators, Including Mutual Irradiation Between Radiator Elements", Journal of the Aerospace Sciences, vol. 29, pp. 1291-1299, 1962.

3. Edwards, J.A. and J.B.Chaddock, "Free Convection and Radiation Heat Transfer from Fin-on-Tube Heat Exchangers", ASME Paper No. 62-WA-205, 1962.

4. Dent, J.C., "An Electrical Network Method for Combined Free Convective and Radiative Transfer From Annular Finned Surfaces", British Chemical Engineering, vol. 13, pp. 90-93, 1968.

5. Keller, H.H. and E.S.Holdredge, "Radiation Heat Transfer for Annular Fins of Trapezoidal Profile", Trans. of the ASME, vol. 92, Series C, pp. 113-116, 1970.

6. Sparrow, E.M. and R.D.Cess, Radiation Heat Transfer, Brooks/Cole Publishing Company, Belmont, California, 1966.

7. Glauz, R.D., "On the Numerical Solution of Ordinary and Partial Differential Equations Using Integral Relations", Journal of the Association for Computing Machinery, vol. 12, pp. 175-180, 1965.

8. Donovan,R.C., Radiation and Convection from Extended Surfaces, Ph.D. Thesis, University of Pittsburgh, 1967.

9. Knudsen, J.G. and R.B.Pan, "Natural Convection Heat Transfer from Transverse Finned Tubes" Chemical Engineering Progress Symposium Series, No. 57, vol. 61, pp. 44-49, 1965.

10. Nwizu, E.I., An Experimental Investigation of Natural Convection Heat Transfer from Isothermal Horizontal Cylinders with Plain Circular Fins, M.S.Thesis, The Ohio State University, 1963.

11. Hamming, R.W., Numerical Methods for Scientists and Engineers, McGraw-Hill Book Company, Inc., New York, 1962, p. 162.

APPENDIX A -- ANGLE FACTORS

The following angle factors were obtained using the standard techniques given in ref. [6].

$$K_{b1}(\tau_b, \rho_1) = \frac{1}{\pi}\left\{\frac{\theta_1 \tan\alpha}{2N_R} - \left[\frac{(d_1b_1 - a_1c_1)a_1 - e_1b_1^2}{N_R(a_1^2 - b_1^2)}\right]\frac{\sin\theta_1}{(a_1 + b_1\cos\theta_1)}\right.$$
$$\left. + \left[\frac{4\rho_1(a_1c_1 + a_1e_1 - d_1b_1)}{a_1^2 - b_1^2} - \frac{a_1\tan\alpha}{N_R}\right]\frac{\tan^{-1}\Omega_1}{\sqrt{a_1^2 - b_1^2}}\right\}$$
$$= dF(\tau_b, \rho_1)dA_b^* - dA_1/d\rho_1 \qquad \text{(A1)}$$

where

$$\tau_o = N_L - \left(1 - \frac{N_R^2}{\rho_1}\right)\tan\alpha$$

$$\theta_1 = \cos^{-1}\left(N_R/\rho_1\right) \qquad \text{if} \quad \tau_b \le \tau_o$$

$$\theta_1 = \cos^{-1}\left(\frac{\tau_b + \tan\alpha - N_L}{N_R\tan\alpha}\right) \qquad \text{if} \quad \tau_b > \tau_o$$

$$\tau_1 = N_L - (1 - \rho_1)\tan\alpha$$

$$a_1 = \rho_1^2 + N_R^2 + (\tau_1 - \tau_b)^2$$

$$b_1 = -2\rho_1 N_R$$

$$c_1 = \rho_1 N_R \tan\alpha$$

$$d_1 = \rho_1(\tau_1 - \tau_b) - (\rho_1^2 + N_R^2)\tan\alpha$$

$$e_1 = \rho_1 N_R \tan\alpha - N_R(\tau_1 - \tau_b)$$

$$\Omega_1 = \frac{(a_1 - b_1)\tan(\theta_1/2)}{\sqrt{a_1^2 - b_1^2}}$$

$$K_{12}(\rho_1,\rho_2) = \frac{2\rho_2\cos\alpha}{\pi}\left\{\frac{c_2\theta_2}{b_2^2} + \left[\frac{(d_2b_2-a_2c_2)a_2 - e_2b_2^2}{b_2(a_2^2-b_2^2)}\right]\frac{\sin\theta_2}{(a_2+b_2\cos\theta_2)}\right.$$

$$\left. + \left[\frac{a_2c_2+a_2e_2-d_2b_2}{a_2^2-b_2^2} - \frac{a_2c_2}{b_2^2}\right]\frac{2\tan^{-1}\Omega_2}{\sqrt{a_2^2-b_2^2}}\right\}$$

$$= dF(\rho_1,\rho_2)dA_1^*-dA_2/d\rho_2 \qquad \text{(A2)}$$

where

$$\lambda_1 = \left(\frac{N_R^2 - \sqrt{(\rho_1^2-N_R^2)(\rho_2^2-N_R^2)}}{\rho_1\rho_2}\right)\tan\alpha + \frac{[N_L - (2-\rho_2)\tan\alpha]}{\rho_2}$$

$$\lambda_2 = \left(\frac{N_R^2 - \sqrt{(\rho_1^2-N_R^2)(\rho_2^2-N_R^2)}}{\rho_1\rho_2}\right)\tan\alpha + \frac{[N_L - (2-\rho_1)\tan\alpha]}{\rho_1}$$

$$\theta_2 = \cos^{-1}(N_R/\rho_1) + \cos^{-1}(N_R/\rho_2) \quad \text{if} \quad \lambda_1 \geq 0 \quad \text{and} \quad \lambda_2 \geq 0$$

$$\theta_2 = \cos^{-1}\left(\frac{(2-\rho_1)\tan\alpha - N_L}{\rho_1\tan\alpha}\right) \quad \text{if} \quad \lambda_2 \leq \lambda_1$$

$$\theta_2 = \cos^{-1}\left(\frac{(2-\rho_2)\tan - N_L}{\rho_2\tan\alpha}\right) \quad \text{if} \quad \lambda_1 < \lambda_2$$

$$a_2 = \rho_1^2 + \rho_2^2 + [N_L - (2-\rho_1-\rho_2)\tan\alpha]^2$$

$$b_2 = -2\rho_1\rho_2$$

$$c_2 = \rho_1\rho_2\tan^2\alpha$$

$$d_2 = (\rho_1+\rho_2)[N_L-(2-\rho_1-\rho_2)\tan\alpha]\tan\alpha - (\rho_1^2+\rho_2^2)\tan^2\alpha$$

$$e_2 = \rho_1\rho_2\tan^2\alpha - (\rho_1+\rho_2)[N_L-(2-\rho_1-\rho_2)\tan\alpha]\tan\alpha + [N_L-(2-\rho_1-\rho_2)\tan\alpha]^2$$

$$\Omega_2 = \frac{(a_2-b_2)\ \tan\ (\theta_2/2)}{\sqrt{a_2^2-\ b_2^2}}$$

APPENDIX B -- NUMERICAL METHODS

General. The technique for determining the distributions of $Q_1(\xi_1)$, $Q_b(\tau_b)$ and $T_1(\xi_1)$ is to approximate the integrals in eqs. (16), (17) and (19) by numerical quadrature formulas and then solve the resulting set of non-linear algebraic equations by iteration. The method employed here is basically that given by Donovan [8] and the reader is referred to his work for a more complete discussion of the technique.

Simpson's one-third rule is used wherever possible in the form:

$$\int_a^b F(x)dx \approx \Delta x \sum_{i=n_1}^{i=n_2} F(x_i)c(i) \tag{B1}$$

where n_1 and n_2 are odd numbers with $n_2 \geq n_1 + 2$; that is, Simpson's rule is applicable only to a set of double panels, each panel having a width Δx. Also,

$$\Delta x = \frac{b - a}{n_2 - n_1} \tag{B2}$$

$$x_i = a + \Delta x(i-n_1) \qquad n_1 \leq i \leq n_2 \tag{B3}$$

$$c(i) = \begin{cases} 1/3 & i = n_1, n_2 \\ 4/3 & i \text{ even} \\ 2/3 & i \text{ odd} \end{cases} \tag{B4}$$

In equation (B1) the continuous function $F(x)$ is replaced by a set of discrete points, $F(x_i)$, uniformly spaced over the integration interval (b-a). In the present application the fin and base surfaces are subdivided into (N-1) and (M-1) intervals, respectively, as shown in Figure 8. The width

of each interval on the fin is

$$\Delta\rho = \frac{1 - N_R}{N - 1} \tag{B5}$$

and on the base

$$\Delta\tau_b = \frac{[N_L - (1-N_R)\tan\alpha] - (1 - N_R)\tan\alpha}{M - 1}$$

$$= \frac{N_L - 2(1-N_R)\tan\alpha}{M - 1} \tag{B6}$$

Both N and M must be odd numbers.

Numerical Approximation of the Radiation Equations. Consider the application of eq. (B1) to the integral in eq. (16a). It becomes

$$\int_{N_R}^{1} \{\varepsilon[T_1^{*4}(\xi) - T_e^{*4}] - (1-\varepsilon)Q_1(\xi)\}K_{12}(N_R, \xi)d\xi$$

$$\approx \Delta\rho \sum_{J=1}^{J=N} \{\varepsilon[T_1^{*4}(J) - T_e^{*4}] - (1-\varepsilon)Q_1(J)\}K_{12}(1,J)c(J) \tag{B7}$$

where $T_1^*(J)$ and $Q_1(J)$ are the values of $T_1^*(\rho_1)$ and $Q_1(\rho_1)$ at the points

$$\rho_1(J) = N_R + \Delta\rho\,(J-1) \qquad J = 1, 2, 3, \ldots, N$$

The coefficients c(J) are given by (B4) with $n_1 = 1$ and $n_2 = N$.

The function $K_{12}(1,J)$ refers to the exchange between the point I = 1 on fin surface "1" in Figure 8 and the set of points J = 1, 2, 3, ..., N on fin surface "2". This function is plotted in Figure 9 with N = 21. The curves for I = 3 and 5 are also shown. The values of N_R, N_L and α correspond to the configuration shown in Figure 1.

It is noted that $K_{12}(I, J)$ varies quite rapidly for small values of I and J. In fact, for I = 1 the peak in the curve is not well defined by the darkened circles corresponding to the points J = 1, 2 and 3. This can result in significant error in the approximation given in eq. (B7). The accuracy of the approximation can be improved by subdividing the two-panel integration interval $1 \leq J \leq 3$ into the eight-panel interval $1 \leq j \leq 9$ shown in Figure 8. The angle factor is designated as $KK_{12}(I, j)$ and is plotted with the open circles in Figure 9 for I = 1 and 3. This function is, of course, also calculated from eq. (A2).

The remainder of the integrand is a more slowly varying function of ρ_1 and can be satisfactorily approximated at the points j = 1, 2, ..., 9 using the following three-point Lagrange interpolation formula:

$$S(j) = \frac{p(p-1)}{2} f(1) + (1-p^2) f(2) + \frac{p(p+1)}{2} f(3) \qquad (B8)$$

where

$$p = (j - 5)/4 \qquad j = 1, 2, \ldots, 9$$

and

$$f(J) = \epsilon[T_1^{*4}(J) - T_e^{*4}] - (1-\epsilon)Q_1(J) \qquad J = 1,2,3$$

Using this notation the integral in eq. (B7) becomes

$$\int_{N_R}^{1} \{\epsilon[T_1^{*4}(\xi) - T_e^{*4}] - (1-\epsilon)Q_1(\xi)\} K_{12}(N_R, \xi) d\xi$$

$$\approx \frac{\Delta\rho}{4} \sum_{j=1}^{j=9} S(j) KK_{12}(1, j) c(j) +$$

$$+ \Delta\rho \sum_{J=3}^{J=N} \{\varepsilon[T_1^{*4}(J) - T_e^{*4}] - (1-\varepsilon)Q_1(J)\}K_{12}(1,J)c(J) \qquad \text{(B9)}$$

The first summation in eq. (B9) extends the integration over eight panels of width $(\Delta\rho/4)$, that is, from $\xi = N_R$ up to $\xi = N_R + 2\Delta\rho$. The second summation covers $(N - 3)$ panels of width $\Delta\rho$ and completes the integration from $\xi = N_R + 2\Delta\rho$ up to $\xi = 1$. Note that in this case $n_1 = 3$ and $n_2 = N$.

All of the integrals in eqs. (16) and (17) are treated in the same manner, including the special handling of the integration near the "corners". The complete set of equations used to determine the functions $Q_1(\rho_1)$ and $Q_b(\tau_b)$ are as follows:

When $I = 1$:

$$Q_1(1) = \varepsilon[1-T_e^{*4}] - \frac{\Delta\rho}{4} \sum_{j=1}^{j=9} S(j)KK_{12}(1,j)c(j)$$

$$- \Delta\rho \sum_{J=3}^{J=N} \{\varepsilon[T_1^{*4}(J) - T_e^{*4}] - (1-\varepsilon)Q_1(J)\}K_{12}(1,J)c(J)$$

$$- \{\varepsilon[1-T_e^{*4}] - (1-\varepsilon)Q_b(M)\}(1-\sin\alpha)/2 \qquad \text{(B10)}$$

When $I = 2, 3$:

$$Q_1(I) = \varepsilon[T_1^{*4}(I) - T_e^{*4}] - \frac{\Delta\rho}{4} \sum_{j=1}^{j=9} S(j)KK_{12}(I,j)c(j)$$

$$- \Delta\rho \sum_{J=3}^{J=N} \{\varepsilon[T_1^{*4}(J) - T_e^{*4}] - (1-\varepsilon)Q_1(J)\}K_{12}(I,J)c(J) \quad -$$

$$- \frac{\Delta\tau_b \, N_R \cos\alpha}{\rho_1(I)} \sum_{K=1}^{K=M-2} \{\varepsilon[1-T_e^{*4}] - (1-\varepsilon)Q_b(K)\}K_{b1}(K,I)\, c(K)$$

$$- \frac{\Delta\tau_b}{4} \frac{N_R \cos\alpha}{\rho_1(I)} \sum_{k=1}^{k=9} T(k) H K_{b1}(k, I)\, c\,(k) \qquad \text{(B11)}$$

When I = 4, ..., N:

$$Q_1(I) = \varepsilon[T_1^{*4}(I) - T_e^{*4}]$$

$$- \Delta\rho \sum_{J=1}^{J=N} \{\varepsilon[T_1^{*4}(J) - T_e^{*4}] - (1-\varepsilon)Q_1(J)\}K_{12}(I,J)c(J)$$

$$- \Delta\tau_b \frac{N_R \cos\alpha}{\rho_1(I)} \sum_{K=1}^{K=M} \{\varepsilon[1-T_e^{*4}] - (1-\varepsilon)Q_b(K)\}K_{b1}(K,I)c(K) \qquad \text{(B12)}$$

When K = 1:

$$Q_b(1) = \varepsilon[1-T_e^{*4}] - \frac{\Delta\rho}{4} \sum_{i=1}^{i=9} S(i) K K_{b1}(1,i)c(i)$$

$$- \Delta\rho \sum_{I=3}^{I=N} \{\varepsilon[T_1^{*4}(I) - T_e^{*4}] - (1-\varepsilon)Q_1(I)\}K_{b1}(1,I)c(I)$$

$$- \{\varepsilon[1-T_e^{*4}] - (1-\varepsilon)Q_1(1)\}(1-\sin\alpha)/2 \qquad \text{(B13)}$$

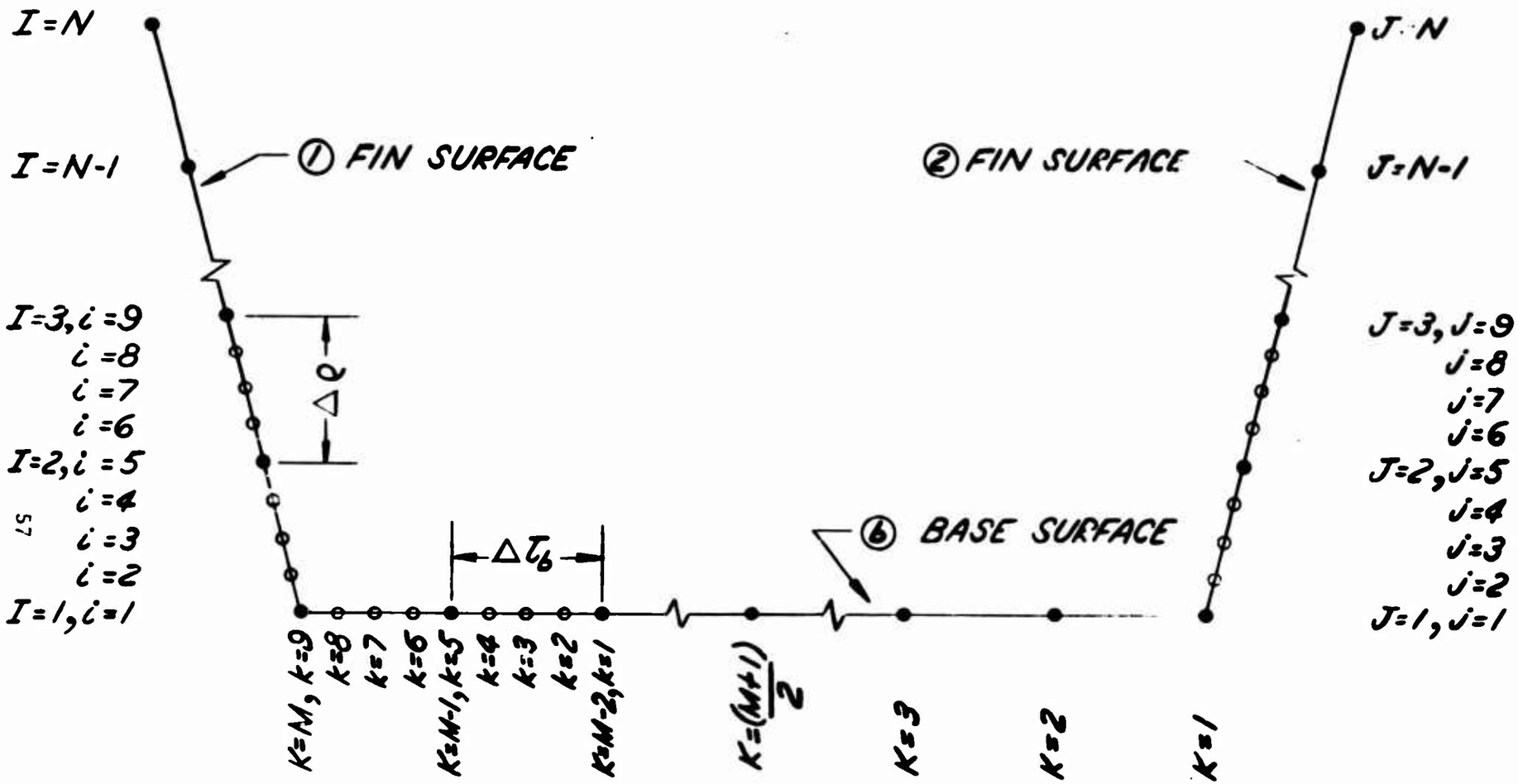

FIGURE 8. POSITION SUBSCRIPTS ON FINS AND ON BASE.

When K = 2, 3:

$$Q_b(K) = \epsilon[1-T_e^{*4}] - \frac{\Delta\ell}{4}\sum_{i=1}^{i=9} S(i)[KK_{b1}(K,i) + KK_{b1}(M+1-K,i)]c(i)$$

$$- \Delta\ell \sum_{I=3}^{I=N} \{\epsilon[T_1^{*4}(I)-T_e^{*4}] - (1-\epsilon)Q_1(I)\}[K_{b1}(K,I) + K_{b1}(M+1-K,I)]c(I)$$

(B14)

When K = 4, ..., (M+1)/2:

$$Q_b(K) = \epsilon[1-T_e^{*4}]$$

$$- \Delta\ell \sum_{I=1}^{I=N} \{\epsilon[T_1^{*4}(I)-T_e^{*4}] - (1-\epsilon)Q_1(I)\}[K_{b1}(K,I)+K_{b1}(M+1-K,I)]c(I)$$

(B15)

Finally, by symmetry, when K = (M+3)/2, ..., M:

$$Q_b(K) = Q_b(M+1-K) \qquad \text{(B16)}$$

In eq. (B11) T(k) is given by

$$T(k) = \frac{p(p-1)}{2} g(M-2) + (1-p^2)g(M-1) + \frac{p(p+1)}{2} g(M)$$

where

$$p = \frac{(k-5)}{4} \qquad k = 1, 2, \ldots, 9$$

$$g(K) = \epsilon(1-T_e^{*4}) - (1-\epsilon)Q_b(K) \qquad K = M-2, M-1, M$$

The functions $HK_{b1}(k,I)$ and $KK_{b1}(K,i)$ are calculated from eq. (A1) at the positions indicated in Figure 8.

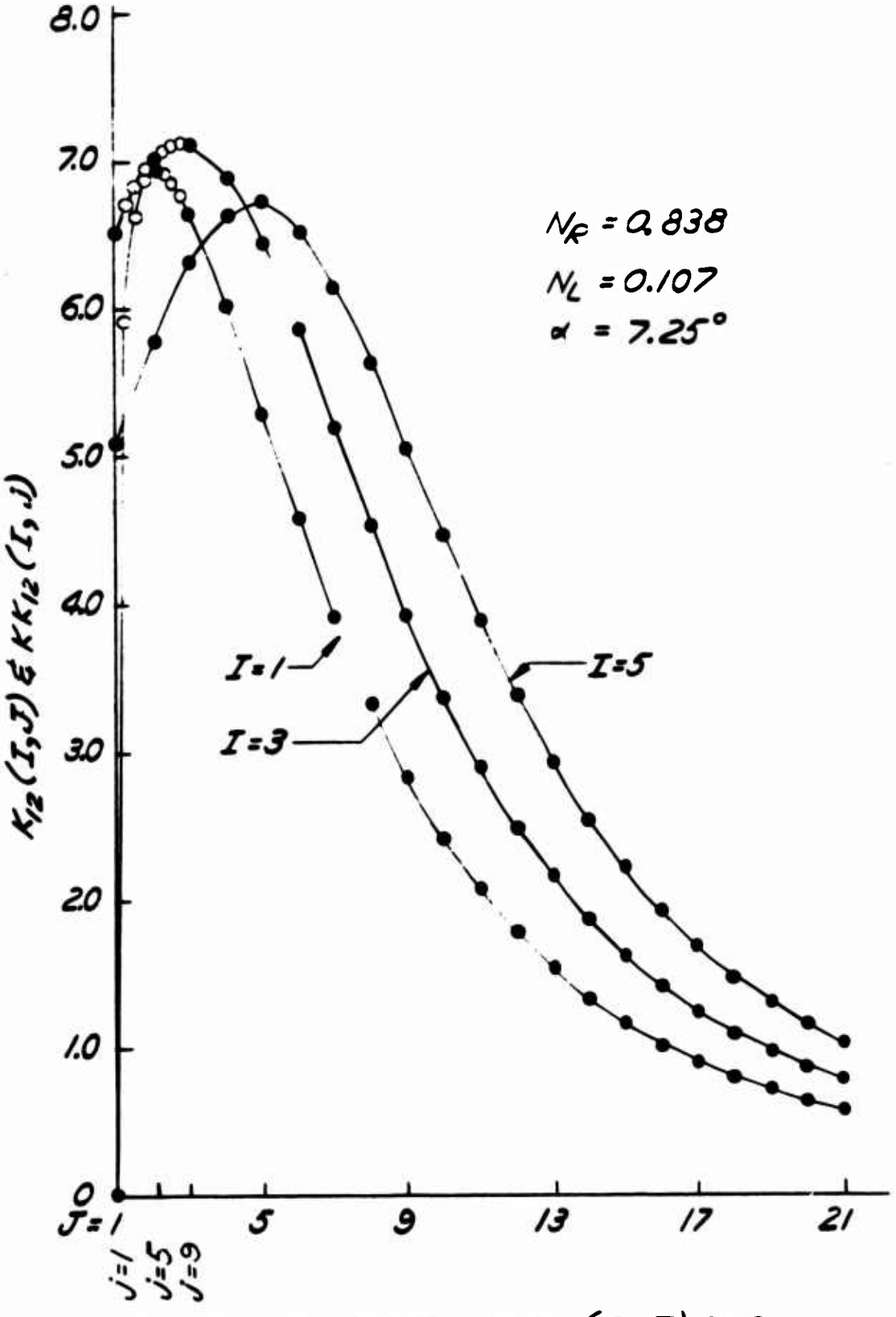

FIGURE 9. PLOT OF $K_{12}(I,J)$ AND $KK_{12}(I,j)$ FOR CONFIGURATION SHOWN IN FIGURE 1.

Numerical Approximation of the Integrated Conduction Equation. The two indefinite integrals in the integrated conduction equation, eq. (19) involve integrating over an odd number of panels of width $\Delta\rho$ when I is an even number and over an even number of panels when I is an odd number. Thus, Simpson's rule can be applied directly to the points $T_I^*(I)$, I = 1,3,5,...,N, but an alternate quadrature formula, applicable to a single panel of width $\Delta\rho$, must be employed at the even numbered points. Donovan [8] uses the following formula from Hamming [11]:

$$\int_{x_i}^{x_i+\Delta x} F(x)dx \approx (\Delta x/24)[9F(x_i) + 19F(x_i+\Delta x) - 5F(x_i+2\Delta x) + F(x_i+3\Delta x)] \quad \text{(B17)}$$

Specializing Simpson's rule to a single interval of width $2\Delta x$ gives

$$\int_{x_i}^{x_i+2\Delta x} F(x)dx \approx (\Delta x/3)[F(x_i) + 4F(x_i+\Delta x) + F(x_i+2\Delta x)] \quad \text{(B18)}$$

Adopting the notation

$$T_A(\rho_1) = \int_{\rho_1}^{1} \psi(\xi)d\xi$$

$$T_B(\rho_1) = \int_{N_R}^{\rho_1} \phi(\xi)d\xi$$

and applying eqs. (B17) and (B18), the conduction equation becomes

$$T_1^*(I) = \frac{1}{P(I)}\left\{[N_R - \rho_1(I)]T_A(I) + T_B(I) + N_R + \frac{[N_R - \rho_1(I)]\delta^* C}{\delta^* + (1-N_R)\tan\alpha}\right\} \tag{B19}$$

where

$$T_A(N) = 0$$

$$T_A(N-1) = (\Delta\rho/24)[9\psi(N) + 19\psi(N-1) - 5\psi(N-2) + \psi(N-3)]$$

When I = N-2, ..., 5, 3, 1

$$T_A(I) = T_A(I+2) + (\Delta\rho/3)[\psi(I) + 4\psi(I+1) + \psi(I+2)]$$

When I = 2, 4, 6, ..., N-3

$$T_A(I) = T_A(I-1) - (\Delta\rho/24)[9\psi(I-1) + 19\psi(I) - 5\psi(I+1) + \psi(I+2)]$$

Also,

$$T_B(1) = 0$$

$$T_B(2) = (\Delta\rho/24)[9\phi(1) + 19\phi(2) - 5\phi(3) - \phi(4)]$$

When I = 3, 5, 7, ..., N

$$T_B(I) = T_B(I-2) + (\Delta\rho/3)[\phi(I) + 4\phi(I-1) + \phi(I-2)]$$

When I = N-1, ..., 8, 6, 4

$$T_B(I) = T_B(I+1) - (\Delta\rho/24)[9\phi(I+1) + 19\phi(I) - 5\phi(I-1) + \phi(I-2)]$$

Note that $T_1^*(1) = 1$ and need not be evaluated from eq. (B19).

Method of Solution. Eqs. (B10) - (B16) and eqs. (B19) represent a set of simultaneous non-linear algebraic equations which are solved by the method of iteration. A weighted average of the two most recent iterates was used to accelerate the convergence. This took the form

$$y_{i+2} = 0.6\, y_i + 0.4\, y_{i+1}$$

where y_{i+1} and y_i are the two most recent iterated values of an unknown and y_{i+2} represents the new estimate.

For the fin configurations studied in this report convergence was usually achieved in less than fifteen iterations. It should be noted, however, that for very tall fins (small values of N_R) or for large temperature drops along the fins (large N_c and h*) the system may converge very slowly or may not converge at all. This difficulty can be circumvented by reducing the values of N_c and h* until a solution is obtained. This solution, along with slightly larger values of N_c and h*, is then fed back into the program as a "first guess" at the new solution. If convergence is achieved the process is repeated until the desired levels of N_c and h* are reached.

In comparing the computed solutions with known solutions of convective and radiative heat transfer from fin systems [1,2] best agreement was found when the step sizes $\Delta\ell$ and $\Delta\tau_b$ were set approximately equal. Using eqs. (B5) and (B6) a guide for choosing N and M is then

$$\frac{M-1}{N-1} \approx \frac{N_L - 2(1-N_R)\tan\alpha}{1-N_R}$$

Usually, a minimum of eleven points was used for either M or N although smaller values can and should be used if the above guide so indicates.

The integrals required in the evaluation of the fin system effectiveness in eq. (24) were found by direct application of Simpson's rule, eq. (B1). The calculation of the actual heat transfer rate from eq. (25) is straightforward. A listing of the computer program is given in Appendix C.

APPENDIX C -- COMPUTER PROGRAM

A list of the major program symbols is given below. The symbol ACC is the accuracy criterion employed in the iteration process. Each time a new value of one of the unknowns $Q_1(I)$, $T_1^*(I)$ or $Q_b(K)$ is calculated its magnitude is compared with its previous value. If the absolute value of the difference is greater than the accuracy criterion, ACC, for any one of the unknowns, a further iteration is calculated. In this study the value ACC = 0.001 was used. The fin angle, ALPHA, must be in radians.

Symbol Used in Program	Symbol Used in Text
ACC	ACC
ALPHA	α
ATB	T_b
C	C
COND	k_m
DELRO	$\Delta\rho$
DELS	δ^*
DELTB	$\Delta\tau_b$
EPS	ϵ
ETA	β
HKB1(K,I)	$HK_{b1}(k,I)$
HS	h^*
K12(I,J)	$K_{12}(I,J)$
KB1(K,I)	$K_{b1}(K,I)$

Symbol Used in Program	Symbol Used in Text
KK12(I,J)	$KK_{12}(I,j)$
KKB1(K,I)	$KK_{b1}(K,i)$
M	M
N	N
NC	N_c
NL	N_L
NR	N_R
P(I)	P(I)
PHI(I)	$\phi(I)$
Q1(I)	$Q_1(I)$
QB(K)	$Q_b(K)$
QC	Q_c
QO	Q_o
QR	Q_R
QT	q_T
RO	R_o
RO1(I)	$\rho_1(I)$
S(J)	S(j)
T(K)	T(k)
TES	T_e^*
T1S(I)	$T_1^*(I)$
X(I)	$\psi(I)$

FLOW CHART OF COMPUTER PROGRAM

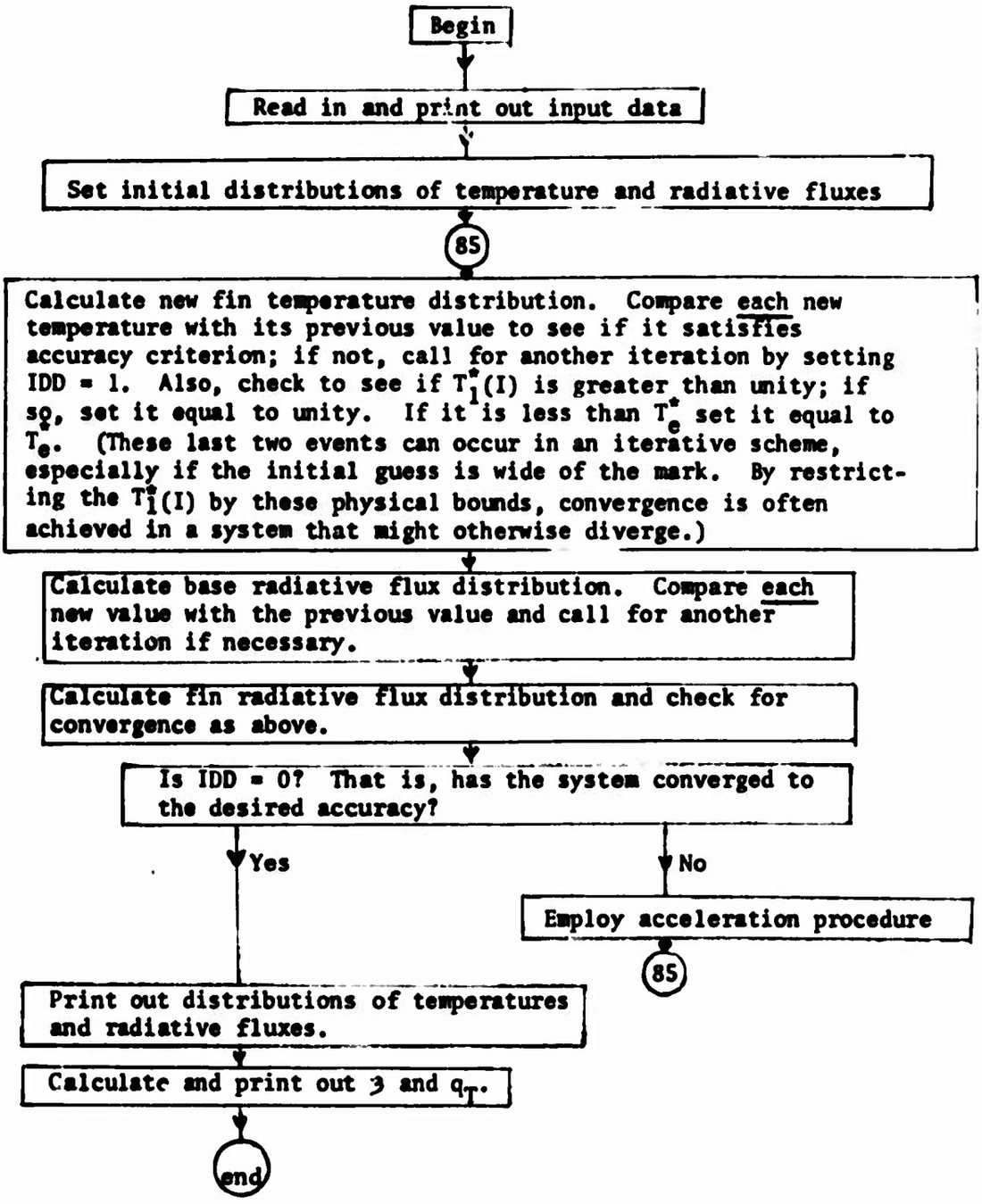

```
C       FORTRAN IV PROGRAM FOR PREDICTING COMBINED CONDUCTION-RADIATION-
C       CONVECTION HEAT TRANSFER FROM ANNULAR FINS OF TRAPEZOIDAL
C       PROFILE ON A CYLINDER.
        REAL NR,NT,NL,NC,K12,KB1,KK12,KKB1
        COMMON KOUNT,IKNT,TES,EPS,M,JSAV,Q1(35),QB(35),T1S(35)
        COMMON K12(35,35),KB1(35,35),RO1(35),RO2(35),TB(35),CS,PI
        COMMON KK12(3,9),KK61(35,9),HKB1(9,3),S(9),T(9),NR,NT,NL
        DIMENSION TA(35),P(35),X(35),PHI(35),A(35),B(35)
        INTEGER READER,PRINT
        READER=5
        PRINT=6
        PI=3.1415927
C       IN THE FOLLOWING READ STATEMENT N MUST BE AN ODD NUMBER EQUAL TO
C       OR GREATER THAN 5 BUT NOT GREATER THAN 35.  M MUST BE AN ODD
C       NUMBER EQUAL TO OR GREATER THAN 7 BUT NOT GREATER THAN 35.
C       THE FIN ANGLE, ALPHA, MUST BE IN RADIANS.
    1   READ(READER,5)N,M,NR,ALPHA,NL,DELS,NC,EPS,HS,TES,ACC
    5   FORMAT(2I4,9F7.0)
C       IN THE FOLLOWING READ STATEMENT RO IS THE FIN-TIP RADIUS IN FEET,
C       ATB IS THE ABSOLUTE VALUE OF THE TUBE TEMPERATURE IN DEGREES
C       RANKINE AND COND IS THE MATERIAL THERMAL CONDUCTIVITY IN
C       BTU/HR-FT-R.
        READ(READER,4)RO,ATB,COND
    4   FORMAT(3F10.0)
        NT=TAN(ALPHA)
        CS=COS(ALPHA)
        WRITE(PRINT,1278)
        WRITE(PRINT,1279)N,M
        WRITE(PRINT,1280)NR
        WRITE(PRINT,1281)ALPHA
        WRITE(PRINT,1282)NL
        WRITE(PRINT,1283)DELS
        WRITE(PRINT,1284)NC
        WRITE(PRINT,1285)EPS
```

```
      WRITE(PRINT,1286)HS
      WRITE(PRINT,1287)TES
      WRITE(PRINT,1288)ACC
      WRITE(PRINT,1289)RO
      WRITE(PRINT,1290)ATB
      WRITE(PRINT,1291)COND
 1278 FORMAT(1H1)
 1279 FORMAT(2X,3HN =,I5,3X,3HM =,I5)
 1280 FORMAT(2X,7HNR     =,F12.6)
 1281 FORMAT(2X,7HALPHA  =,F12.6)
 1282 FORMAT(2X,7HNL     =,F12.6)
 1283 FORMAT(2X,7HDELS   =,F12.6)
 1284 FORMAT(2X,7HNC     =,F12.6)
 1285 FORMAT(2X,7HEPS    =,F12.6)
 1286 FORMAT(2X,7HHS     =,F12.6)
 1287 FORMAT(2X,7HTES    =,F12.6)
 1288 FORMAT(2X,7HACC    =,F12.6)
 1289 FORMAT(2X,7HRO     =,F12.6,4H  FT)
 1290 FORMAT(2X,7HATB    =,F12.6,17H  DEGREES RANKINE)
 1291 FORMAT(2X,7HCOND   =,F12.6,13H  BTU/HR-FT-R)
      XN=N-1
      XM=M-1
      DELRO=(1.-NR)/XN
      DELTB=(NL-2.*NT*(1.-NR))/XM
      DO 3 I=1,N
      XI=I-1
      RO1(I)=NR +XI*DELRO
    3 RO2(I)=RO1(I)
C     CALCULATION OF MATRIX K12(I,J)
      DO 2 I=1,N
      DO 2 J=1,N
      CALL MK12(I,J,ANG)
    2 K12(I,J)=ANG
```

```
      DO 9 J=1,9
      XJ=J-1
    9 RO2(J)=NR+XJ*(DELRO/4.)
C     CALCULATION OF MATRIX KK12(I,J)
      DO 10 I=1,3
      DO 10 J=1,9
      CALL MK12(I,J,ANG)
   10 KK12(I,J)=ANG
      KK12(1,1)=0.0
C     CALCULATION OF MATRIX HKB1(K,I)
      M1=M-8
      M2=M-1
      DO 14 K=M1,M2
      XK=M-K
      TB(K)=NL-(1.-NR)*NT -XK*(DELTB/4.)
      DO 14 I=2,3
      CALL MKB1(K,I,ANG)
      KK=K +9 -M
   14 HKB1(KK,I)=ANG
      HKB1(9,2)=0.0
      HKB1(9,3)=0.0
      DO 11 K=1,M
      XK=K-1
   11 TB(K)=(1.-NR)*NT +XK*DELTB
C     CALCULATION OF MATRIX KB1(K,I)
      MM=M-1
      DO 20 K=1,MM
      DO 20 I=2,N
      CALL MKB1(K,I,ANG)
   20 KB1(K,I)=ANG
      DO 50 K=1,M
   50 KB1(K,1)=0.0
      DO 55 I=1,N
```

```
   55 KB1(M,I)=0.0
      DO 7 I=2,9
      XI=I-1
    7 RO1(I)=NR +XI*(DELRO/4.)
C     CALCULATION OF MATRIX KKB1(K,I) FOR K=1,2,3
      DO 12 K=1,3
      DO 12 I=2,9
      CALL MKB1(K,I,ANG)
   12 KKB1(K,I)=ANG
      KKB1(1,1)=0.0
      KKB1(2,1)=0.0
      KKB1(3,1)=0.0
C     CALCULATION OF MATRIX KKB1(K,I) FOR K=M-2,M-1
      M1=M-2
      M2=M-1
      DO 13 K=M1,M2
      DO 13 I=2,9
      CALL MKB1(K,I,ANG)
   13 KKB1(K,I)=ANG
      KKB1(M1,1)=0.0
      KKB1(M2,1)=0.0
C     SET INITIAL DISTRIBUTIONS OF TEMPERATURE AND RADIATIVE FLUXES
      BT=DELS+(1.-NR)*NT
      DO 80 I=1,N
      TIS(I)=1.0
      A(I)=1.0
      C1(I)=0.5
      B(I)=0.5
      XI=I-1
      RO1(I)=NR +XI*DELRO
   80 P(I)= RO1(I)*(DELS +(1.-RO1(I))*NT)/BT
      DO 82 I=1,M
   82 QB(I)=0.5
```

```
      ITER=0
C     CALCULATION OF FIN TEMPERATURE DISTRIBUTION
   85 C=(HS*(TIS(N)-TES) +EPS*NC*(TIS(N)**4-TES**4))*(BT*CS/NR**2)
      ITER=ITER+1
      IF (ITER-30)86,86,1041
 1041 WRITE(PRINT,1042)
 1042 FORMAT(///2X,85HCONVERGENCE NOT ACHIEVED AFTER 30 ITERATIONS.  INC
     1REASE ACC OR DECREASE NC AND/OR HS.)
      GO TO 135
   86 IDD=0
      DO 88 I=1,N
      X(I)=RO1(I)*(NC*Q1(I)+HS*(TIS(I)-TES))/NR**2
      TEM1=(DELS+NT-2.*NT*RO1(I))/BT
      TEM2=(NR-RO1(I))
   88 PHI(I)=TIS(I)*TEM1+TEM2*X(I)
      TA(N)=0.0
      TA(N-1)=DELRO/24.*(9.*X(N)+19.*X(N-1)-5.*X(N-2)+X(N-3))
      NN=N-2
70    DO 90 I=1,NN,2
      NI1=N-I-1
   90 TA(NI1)=TA(NI1+2)+DELRO/3.*(X(NI1)+4.*X(NI1+1)+X(NI1+2))
      NN=N-3
      DO 93 I=2,NN,2
   93 TA(I)=TA(I-1)-DELRO/24.*
     1(9.*X(I-1)+19.*X(I)-5.*X(I+1)+X(I+2))
      TB(1)=0.0
      TB(2)=DELRO/24.*(9.*PHI(1)+19.*PHI(2)-5.*PHI(3)+PHI(4))
      DO 94 I=3,N,2
   94 TB(I)=TB(I-2)+DELRO/3.*(PHI(I)+4.*PHI(I-1)+PHI(I-2))
      NN=N-4
      DO 96 I=1,NN,2
      NI1=N-I
   96 TB(NI1)=TB(NI1+1)-DELRO/24.*(9.*PHI(NI1+1)+19.*PHI(NI1)-5.*PHI(NI1
```

```
     1-1)+PHI(N11-2))
      DO 98 I=2,N
      AA=T1S(I)
      T1S(I)=(1./P(I))*((NR-RO1(I))*TA(I) +TB(I) +NR
     1+(NR-RO1(I))*DELS*C/BT)
 6010 IF (ABS(T1S(I)-AA).LE.ACC) GO TO 6015
      ICO=1
 6015 IF(T1S(I).LE.1.0.AND.T1S(I).GT.TES) GO TO 98
      IF(T1S(I).GT.1.0    ) GO TO 91
      T1S(I)=TES
      GO TO 98
   91 T1S(I)=1.0
   98 CONTINUE
C     CALCULATION OF BASE RADIATIVE FLUX DISTRIBUTION
      DO 1050 I=1,9
      XI=I-5
      PP=XI/4.
      TEM1=PP*(PP-1.)/2.*(EPS*(1.-TES**4)-(1.-EPS)*Q1(1))
      TEM2=(1.-PP**2)*(EPS*(T1S(2)**4-TES**4)-(1.-EPS)*Q1(2))
      TEM3=PP*(PP+1.)/2.*(EPS*(T1S(3)**4-TES**4)-(1.-EPS)*Q1(3))
 1050 S(I)=TEM1+TEM2+TEM3
      TEM1=EPS*(1.-TES**4)
      TEM2=(1.-EPS)*Q1(1)
      TEM3=(1.-SIN(ALPHA))/2.
      KOUNT=8
      IKNT=1
      NN=N-3
      TEM6=NR+2.*DELRC
      CALL SIMP(NR,TEM6,8,TEM4)
      IKNT=3
      KOUNT=4
      CALL SIMP(TEM6,1.0,NN,TEM5)
      AA=QB(1)
```

```
      QB(1)=TEM1-(TEM1-TEM2)*TEM3-(TEM4+TEM5)
      IF (ABS(QB(1)-AA).LE.ACC) GO TO 110
      ICD=1
  110 MM=(M+1)/2
      DO 115 K=2,MM
      AA=QB(K)
      JSAV=K
      IF (K.GT.3) GO TO 1060
      KOUNT=9
      IKNT=1
      CALL SIMP(NR,TEM6,8,TEM2)
      KOUNT=5
      IKNT=3
      CALL SIMP(TEM6,1.0,NN,TEM3)
      QB(K)=TEM1-TEM2-TEM3
      GO TO 1065
 1060 KOUNT=5
      NN=N-1
      IKNT=1
      CALL SIMP(NR,1.0,NN,TEM2)
      QB(K)=TEM1-TEM2
 1065 IF (ABS(QB(K)-AA).LE.ACC) GO TO 115
      IDD=1
  115 CONTINUE
      MM=(M+3)/2
      DO 116 K=MM,M
      NI1=M+1-K
  116 QB(K)=QB(NI1)
C     CALCULATION OF FIN RADIATIVE FLUX DISTRIBUTION
      DO 1051 I=1,9
      XI=I-5
      PP=XI/4.
      TEM1=PP*(PP-1.)/2.*(EPS*(1.-TES**4)-(1.-EPS)*QB(M-2))
```

```
      TEM2=(1.-PP**2)*(EPS*(1.-TES**4)-(1.-EPS)*QB(M-1))
      TEM3=PP*(PP+1.)/2.*(EPS*(1.-TES**4)-(1.-EPS)*QB(M))
1051  T(1)=TEM1+TEM2+TEM3
      TEM1=EPS*(1.-TES**4)
      TEM2=(1.-EPS)*QB(M)
      TEM6=NR+2.*DELRO
      JSAV=1
      KOUNT=10
      IKNT=1
      CALL SIMP(NR,TEM6,8,TEM4)
      IKNT=3
      NN=N-3
      KOUNT=6
      CALL SIMP(TEM6,1.0,NN,TEM5)
      AA=Q1(1)
      TEM3=(1.-SIN(ALPHA))/2.
      Q1(1)=TEM1-TEM4-TEM5-(TEM1-TEM2)*TEM3
      IF (ABS(Q1(1)-AA).LE.ACC) GO TO 120
      IDD=1
120   TEM4=NT*(1.-NR)
      TEM8=NL-NT*(1.-NR)-2.*DELTB
      TEM9=NL-NT*(1.-NR)
      DO 130 I=2,N
      JSAV=I
      AA=Q1(I)
      TEM1=EPS*(T1S(I)**4-TES**4)
      TEM2=(NR*CS)/RO1(I)
      IF (I.GT.3) GO TO 1070
      KOUNT=10
      IKNT=1
      CALL SIMP(NR,TEM6,8,TEM3)
      KOUNT=6
      IKNT=3
```

```
      NN=N-3
      CALL SIMP(TEM6,1.0,NN,TEM7)
      KOUNT=7
      IKNT=1
      MM=M-3
      CALL SIMP(TEM4,TEM8,MM,TT1)
      IKNT=1
      KOUNT=11
      CALL SIMP(TEM8,TEM9,8,TT2)
      Q1(I)=TEM1-TEM3-TEM7-TEM2*(TT1+TT2)
      GO TO 1075
 1070 KOUNT=6
      IKNT=1
      NN=N-1
      CALL SIMP(NR,1.0,NN,TEM3)
      IKNT=1
      KOUNT=7
      MM=M-1
      CALL SIMP(TEM4,TEM9,MM,TT1)
      Q1(I)=TEM1-TEM3-TEM2*TT1
 1075 IF (ABS(Q1(I)-AA).LE.ACC) GO TO 130
      ICO=1
  130 CONTINUE
      IF(ICO.EQ.0) GO TO 135
C     ACCELERATION PROCEDURE
      DO 5810 I=2,N
      T1S(I)=0.6*A(I) +0.4*T1S(I)
      A(I)=T1S(I)
      Q1(I)=0.6*B(I) +0.4*Q1(I)
 5810 B(I)= Q1(I)
      GO TO 85
C     PRINT-OUT ROUTINE
  135 WRITE(PRINT,136)
```

```
  136 FORMAT(///2X,69HFIN TEMPERATURE DISTRIBUTION          FIN RADIATIV
     1E FLUX DISTRIBUTION//)
      WRITE(PRINT,138)(I,T1S(I),I,Q1(I),I=1,N)
  138 FORMAT(4X,4HT1S(,I2,3H) =,E15.7,16X,3HQ1(,I2,3H) =,E15.7)
      WRITE(PRINT,1278)
      WRITE(PRINT,139)
  139 FORMAT(2X,32HBASE RADIATIVE FLUX DISTRIBUTION//)
      WRITE(PRINT,141)(I,QB(I),I=1,M)
  141 FORMAT(4X,3HQB(,I2,3H) =,E15.7)
C     CALCULATION OF ETA AND QT
      KOUNT=1
      NN=N-1
      MM=M-1
      IKNT=1
      CALL SIMP(NR,1.0,NN,XIQ1)
      KOUNT=2
      IKNT=1
      CALL SIMP(TEM4,TEM9,MM,XIQB)
      KOUNT=3
      IKNT=1
      CALL SIMP(NR,1.0,NN,XIT1)
      QR=(2./CS)*XIQ1  +2.*DELS*EPS*(T1S(N)**4-TES**4) +NR*XIQB
      QC=(2./CS)*XIT1 +2.*DELS*(T1S(N)-TES) +NR*(1.-TES)*
     1(NL-2.*(1.-NR)*NT)
      QO=NR*(NL+2.*DELS)*(EPS*NC*(1.-TES**4) +HS*(1.-TES))
      ETA=(NC*QR +HS*QC)/QO
      QT=(2.*PI*ETA*QO/NR**2)*(RO*ATB*CCND*CS)*BT
      WRITE(PRINT,150)ETA
  150 FORMAT(////2X,33HFIN SYSTEM EFFECTIVENESS -- ETA =,E15.7)
      WRITE(PRINT,151)QT
  151 FORMAT(///2X,32HTOTAL HEAT TRANSFER RATE -- QT =,E15.7,8H  BTU/HR)
      END
```

```
      SUBROUTINE MK12(I,J,ANG)
      REAL NR,NT,NL,NC,K12,KB1,KK12,KKB1
      COMMON KOUNT,IKNT,TES,EPS,M,JSAV,G1(35),GB(35),T1S(35)
      COMMON K12(35,35),KB1(35,35),RO1(35),RO2(35),TB(35),CS,PI
      COMMON KK12(3,9),KKB1(35,9),HKB1(9,3),S(9),T(9),NR,NT,NL
      TEM1= NR**2 -SQRT((RO1(I)**2 -NR**2)*(RO2(J)**2-NR**2))
      TEM1=(TEM1*NT)/(RO1(I)*RO2(J))
      ALAM1=TEM1 +(NL-(2.-RO2(J))*NT)/RO2(J)
      ALAM2=TEM1 +(NL-(2.-RO1(I))*NT)/RO1(I)
      IF(ALAM1.GE.0.0.AND.ALAM2.GE.0.0) GO TO 15
      IF(ALAM2.LE.ALAM1)GO TO 17
      THETA2=ARCOS(((2.-RO2(J))*NT-NL)/(RO2(J)*NT))
      GO TO 20
   17 THETA2=ARCOS(((2.-RO1(I))*NT-NL)/(RO1(I)*NT))
      GO TO 20
   15 COM1=NR/RO1(I)
      COM2=NR/RO2(J)
      ARCS1=0.0
      ARCS2=0.0
      IF (COM1.NE.1..AND.COM2.NE.1.) GO TO 68
      IF (COM1.EQ.1..AND.COM2.EQ.1.) GO TO 70
      IF (COM1.EQ.1.) GO TO 69
      ARCS1=ARCOS(COM1)
      GO TO 70
   68 ARCS1=ARCOS(COM1)
   69 ARCS2=ARCOS(COM2)
   70 THETA2=ARCS1+ARCS2
   20 TEM1= NL-(2.-RO1(I)-RO2(J))*NT
      A2=RO1(I)**2 +RO2(J)**2 +TEM1**2
      B2=-2.*RO1(I)*RO2(J)
      C2=RO1(I)*RO2(J)*NT**2
      D2=(RO1(I) +RO2(J))*TEM1*NT -(RO1(I)**2 +RO2(J)**2)*NT**2
      E2=RO1(I)*RO2(J)*NT**2 -(RO1(I)+RO2(J))*TEM1*NT  +TEM1**2
```

```
OMEGA2 =((A2- B2)*TAN(THETA2/2.))/SQRT(A2**2-B2**2)
TEM1=((D2*B2-A2*C2)*A2 -E2*B2**2)/(B2*(A2**2-B2**2))
TEM1=(TEM1*SIN(THETA2))/(A2 +B2*COS(THETA2))
TEM2=(A2*C2 +A2*E2 -D2*B2)/(A2**2-B2**2) -(A2*C2)/B2**2
TEM2=(TEM2*2.*ATAN( OMEGA2))/SQRT(A2**2-B2**2)
ANG      =(2.*RO2(J)*CS/PI)*((C2*THETA2)/B2**2 +TEM1 +TEM2)
RETURN
END
```

```
      SUBROUTINE MKB1(K,I,ANG)
      REAL NR,NT,NL,NC,K12,KB1,KK12,KKB1
      COMMON KOUNT,IKNT,TES,EPS,M,JSAV,C1(35),QB(35),TLS(35)
      COMMON K12(35,35),KB1(35,35),RO1(35),RO2(35),TB(35),CS,PI
      COMMON KK12(3,9),KKB1(35,9),HKB1(9,3),S(9),T(9),NR,NT,NL
      TO=NL-(1.-NR**2/RO1(I))*NT
      IF(TB(K).LE.TO) GO TO 58
      THETA1=ARCOS((TB(K) +NT -NL)/(NR*NT))
      GO TO 60
   58 THETA1=ARCOS(NR/RO1(I))
   60 T1=NL-(1.-RO1(I))*NT
      A1=RO1(I)**2 +NR**2 +(T1-TB(K))**2
      B1=-2.*RO1(I)*NR
      C1=RO1(I)*NR*NT
      D1=RO1(I)*(T1-TB(K))-(RO1(I)**2 +NR**2)*NT
      E1=RO1(I)*NR*NT -NR*(T1-TB(K))
      OMEGA1 =((A1-B1)*TAN(THETA1/2.))/SQRT(A1**2-B1**2)
      TEM1=((D1*B1-A1*C1)*A1 -E1*B1**2)/(NR*(A1**2-B1**2))
      TEM1=(TEM1*SIN(THETA1))/(A1 +B1*COS(THETA1))
      TEM2=(4.*RO1(I)*(A1*C1 +A1*E1 -D1*B1))/(A1**2-B1**2) -(A1*NT)/NR
   78 TEM2=(TEM2*ATAN( OMEGA1))/SQRT(A1**2-B1**2)
      ANG      =(1./PI)*((THETA1*NT/(2.*NR))-TEM1 +TEM2)
      RETURN
      END
```

```
      SUBROUTINE SIMP(A,B,N,YI)
      REAL NR,NT,NL,NC,K12,KB1,KK12,KKB1
      COMMON KOUNT,IKNT,TES,EPS,M,JSAV,Q1(35),QB(35),T1S(35)
      COMMON K12(35,35),KB1(35,35),RO1(35),RO2(35),TB(35),CS,PI
      COMMON KK12(3,9),KKB1(35,9),HKB1(9,3),S(9),T(9),NR,NT,NL
      DX=(B-A)/FLOAT(N)
      YI=FUN(A)
      X=A+DX
      K=1
      NN=N-1
      DO 2 I=1,NN
      IKNT=IKNT+1
      Y=FUN(X)
      GO TO (4,6),K
    4 YI=4.*Y+YI
      K=2
      GO TO 2
    6 YI=2.*Y+YI
      K=1
    2 X=X+DX
      IKNT=IKNT+1
      Y=FUN(X)
      YI=DX*(YI+Y)/3.
      RETURN
      END
```

```
      FUNCTION FUN(X)
      REAL NR,NT,NL,NC,K12,KB1,KK12,KKB1
      COMMON KOUNT,IKNT,TES,EPS,M,JSAV,Q1(35),QB(35),T1S(35)
      COMMON K12(35,35),KB1(35,35),RO1(35),RO2(35),TB(35),CS,PI
      COMMON KK12(3,9),KKB1(35,9),HKB1(9,3),S(9),T(9),NR,NT,NL
      GO TO (10,20,30,40,50,60,70,80,90,100,110),KOUNT
   10 FUN=Q1(IKNT)*X
      RETURN
   20 FUN=QB(IKNT)
      RETURN
   30 FUN=(T1S(IKNT)-TES)*X
      RETURN
   40 FUN=(EPS*(T1S(IKNT)**4-TES**4)-(1.-EPS)*Q1(IKNT))*KB1(1,IKNT)
      RETURN
   50 S1=EPS*(T1S(IKNT)**4-TES**4)-(1.-EPS)*Q1(IKNT)
      II=M+1-JSAV
      S2=KB1(JSAV,IKNT)+KB1(II,IKNT)
      FUN=S1*S2
      RETURN
   60 FUN=(EPS*(T1S(IKNT)**4-TES**4)-(1.-EPS)*Q1(IKNT))*K12(JSAV,IKNT)
      RETURN
   70 FUN=(EPS*(1.-TES**4)-(1.-EPS)*QB(IKNT))*KB1(IKNT,JSAV)
      RETURN
   80 FUN=S(IKNT)*KKB1(1,IKNT)
      RETURN
   90 II=M+1-JSAV
      FUN=S(IKNT)*(KKB1(JSAV,IKNT)+KKB1(II,IKNT))
      RETURN
  100 FUN=S(IKNT)*KK12(JSAV,IKNT)
      RETURN
  110 FUN=T(IKNT)*HKB1(IKNT,JSAV)
      RETURN
      END
```